Journal of Power Sources 194 (2009) 130–145

Contents lists available at ScienceDirect

Journal of Power Sources

journal homepage: www.elsevier.com/locate/jpowsour

Review

A review on polymer electrolyte membrane fuel cell catalyst degradation and starvation issues: Causes, consequences and diagnostic for mitigation

N. Yousfi-Steiner[a,b], Ph. Moçotéguy[a,*], D. Candusso[c,b], D. Hissel[b]

[a] EIFER, European Institute For Energy Research, Emmy-Noether Strasse 11, 76131 Karlsruhe, Germany
[b] FEMTO-ST/ENISYS FCLAB, UMR CNRS 6174, University of Franche-Comté, rue Mieg, 90010 Belfort cedex, France
[c] INRETS/FCLAB, The French National Institute for Transport and Safety Research, rue Mieg, 90010 Belfort cedex, France

ARTICLE INFO

Article history:
Received 23 November 2008
Received in revised form 23 March 2009
Accepted 25 March 2009
Available online 7 April 2009

Keywords:
PEM fuel cell
Diagnosis
Degradation
Starvation
Catalyst
Mixed potential

ABSTRACT

In proton exchange membrane fuel cells, cost, reliability and durability are important issues that need to be solved before their commercialization. Their performance decrease during operation is attributed, amongst others, to the loss of electrochemical surface area occurring during long-term ageing, after transients or after an incident (faulty operation). These losses are mainly due to catalyst metal degradation and carbon-support corrosion, which are continuous irreversible processes that can dramatically reduce the fuel cell lifetime.

In this paper, the phenomena linked to catalyst and carbon-support degradation are reviewed, focusing on those caused by fuel and oxidant starvation, since these faulty conditions are amongst the most critical for fuel cell durability. A description of reactions potentially involved in the catalyst degradation, associated with thermodynamic and kinetic considerations related to fuel cell operation are reviewed. This information is used to interpret the experimental results presented in the literature and reviewed in this paper. Based on these reviews, an analysis of the "reverse decay current mechanism" is performed and an alternative mechanism is suggested together with an experiment that would identify the most likely between them. Finally, some characterization methods or mitigation strategies are listed and an illustrative fault tree is built, pointing out the relationship between causes and symptoms in catalyst degradation.

Contents

1. Introduction 131
2. PEM fuel cell description 131
   2.1. Cell description 131
   2.2. Reactions occurring in PEMFC 132
      2.2.1. Hydrogen adsorption and oxidation 132
      2.2.2. Oxygen reduction and adsorption on platinum 132
      2.2.3. Pt dissolution and reprecipitation 133
      2.2.4. Carbon corrosion 133
   2.3. Thermodynamics of PEMFC 133
   2.4. Kinetic considerations 134
      2.4.1. Overview of electrochemical kinetics 134
      2.4.2. Kinetics of oxygen reactions at Pt electrodes 134
   2.5. Considerations about mixed potentials 135
3. Long-term catalyst and carbon-support degradations 136
4. Starvation 136
   4.1. Causes and consequences of starvation 136

* Corresponding author. Tel.: +49 721 610 513 37; fax: +49 721 610 513 32.
E-mail addresses: nadia.steiner@eifer.org (N. Yousfi-Steiner), philippe.mocoteguy@eifer.org (Ph. Moçotéguy), denis.candusso@inrets.fr (D. Candusso), daniel.hissel@univ-fcomte.fr (D. Hissel).

0378-7753/$ – see front matter © 2009 Elsevier B.V. All rights reserved.
doi:10.1016/j.jpowsour.2009.03.060

4.2. Fuel starvation 137
4.2.1. Local fuel starvation 137
4.2.2. Overall starvation 141
4.3. Oxidant starvation 141
5. Failure prevention 141
5.1. Fault tree analysis 141
5.2. Existing diagnostic methods 142
5.3. Mitigation, prevention 143
6. Conclusion 143
Acknowledgements 144
References 144

Nomenclature

a_x	activity of the specie x
E	potential (V)
F	Faraday constant, 96.487 (C mol^{-1})
G	Gibbs free energy (J)
i	current (A)
j	current density (A cm^{-2})
P_x	partial pressure of the specie x (Pa)
r	ohmic resistance (Ω)
R	gas constant, 8.314472 (J mol^{-1} K^{-1})
S	entropy (J K^{-1})
T	temperature (K)
U	voltage (V)
z_i	charge number of the specie i

Greek letters

μ	chemical potential (J mol^{-1})
$\tilde{\mu}$	electrochemical potential (J mol^{-1})
$\eta_.$	electrode polarization (V)
α	transfer coefficient
ν	stoichiometry coefficient
φ	Galvani potential (V)

Subscripts, superscripts

m	metal
s	solution
ox	oxidant
red	reducer
mix	mixed
eq	equivalent
lim	limiting
a	anode
c	cathode

1. Introduction

Reliability, cost and durability appear to be the most important considerations to successfully achieve the commercialization of polymer electrolyte membrane fuel cell (PEMFC). Indeed, the minimum lifetime requirements set by the American Department of Energy (DoE) for 2010 are 40,000 h for stationary applications (which is equivalent to 5 years of continuous operation) and about 5000 h for automotive [1].

Fuel cells are prone to chemical, mechanical or thermal degradation [2–16] and three degradation classes could be distinguished: "baseline degradation", degradation due to transients and incident-induced degradation. All these degradation classes induce fuel cell voltage/performance decrease and lifetime reduction. The baseline degradation is due to long-term material degradation. It is irreversible, unavoidable and exists as long as the fuel cell is operating. The second degradation class is linked to the cycling or variation of operating conditions; it is induced by temperature, humidity and/or voltage cycling. Finally, sudden degradation happens when the fuel cell is subjected to detrimental operating conditions such as fuel starvation.

In general, PEMFC lifetime can be reduced by bad water management [6,14,17–19], membrane electrode assembly (MEA) (and especially catalyst) contamination by impurities [15,18,20], power and/or thermal cycling. All can in turn induce MEA degradation, Pt dissolution and agglomeration [21–27] or carbon corrosion [5,11,12,28–32]. Conversely, severe degradation occur under uncontrollable anomalies (oxygen permeation through the membranes...) or under faulty control of operating parameters, such as reactant starvation (and above all, fuel starvation), which refers to an operation with an insufficient amount of gas in the active layer [8,9,31,33–40].

A huge effort is thus made worldwide to understand the degradation mechanisms so as to achieve the lifetime objectives addressed above. Due to the wide scope of this subject and the several review papers already published on the effect of contaminants [15,18,20] and water management [6,14,18,41,42], this paper will only review the degradation mechanisms associated with Pt catalyst and carbon support and will specifically focus on fuel and oxidant starvations.

In addition, regarding cost, the needed amount of the Pt in a fuel cell has drawn a long reduction race from 28 mg cm^{-2} in the early days [43] to 0.4 mg cm^{-2} or less at the cathode and 0.05 mg cm^{-2} at the anode in 2006 [44]. This was achieved by progressively replacing pure Pt black by carbon-support Pt nanoparticles. Therefore, degradations of both carbon and platinum are linked and reinforce each other. On the one hand, platinum catalyzes the carbon-support oxidation [5,44,45] and on the other hand carbon-support oxidation accelerates the release of supported catalyst particles and therefore active surface area loss [5,44].

This paper's second section gives a complete description of PEMFC including all reactions involving platinum, carbon support and reactants; it gathers the basic knowledge needed to understand Pt and carbon-support degradation. In the third and fourth sections, literature results dealing respectively with long-term operation and reactant starvation are analyzed. Finally, in the fifth section, a fault tree summarizing all the PEMFC electrocatalyst degradations is built in order to reveal the connections between causes and effects as well as existing diagnosis and mitigation methods.

2. PEM fuel cell description

2.1. Cell description

A PEMFC consists of two electrodes in contact with a membrane separating gas compartments (cf. Fig. 1). The membrane is designed as an electronic insulator material separating the reactants (H_2 and O_2/air) and allowing only the "transit" of protons towards the

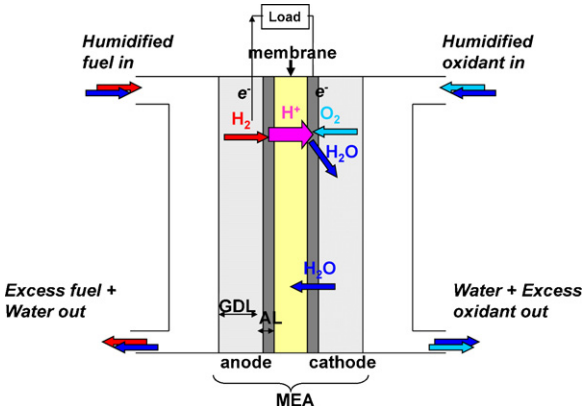

Fig. 1. Basics of PEM fuel cell operation.

electrodes. The electrodes are constituted of a gas diffusion layer (GDL) and an active layer (AL), which both have a porous structure. This assembly is sandwiched between two current collectors, also known as bipolar plates, in which gas distribution channels are integrated.

The GDL is typically cloth or carbon paper (0.2–0.5 mm thickness) that provides rigidity and support to the membrane electrode assembly (MEA). It incorporates hydrophobic material that facilitates the product water drainage and prevents the gas paths from water accumulation.

The AL consists of catalyst particles, ionomer and pore spaces which form a three-phase boundary where electrons, protons and reactant gases meet and electrochemical reaction takes place. A good active layer has to make the trade-off between keeping enough water to guaranty a good protonic conductivity in the ionomeric phase and having an optimal pore size distribution to facilitate produced water evacuation.

Up to now, platinum (pure or alloyed) is the catalyst material which gives the best electrocatalytic performances [46]. In latest generations of PEMFC electrodes, nanoparticles (size in the range of 2–6 nm) of platinum are uniformly dispersed on carbon-support submicrometric particles in order to achieve uniform distribution of the catalyst on the electrode surface, thus maximizing the active surface area [47]. Moreover, carbon support also ensures electronic conductivity and stabilizes the catalyst which is then less subject to agglomeration problems than non-supported catalyst.

As shown in Fig. 1, two oxido-reduction couples are involved in fuel cell's electrochemical energy production: H^+/H_2 at the negative electrode and O_2/H_2O at the positive one. At the negative electrode, which operates as anode, the hydrogen is oxidized according to:

$$H_2 \rightarrow 2H^+ + 2e^- \quad (1)$$

At the positive electrode which operates as cathode, oxygen is reduced according to:

$$O_2 + 4H^+ + 4e^- \rightarrow 2H_2O \quad (2)$$

The global reaction is therefore:

$$2H_2 + O_2 \underset{a}{\overset{b}{\leftrightarrows}} 2H_2O \quad (3)$$

Besides water, the operation of a PEMFC releases electricity and heat.

2.2. Reactions occurring in PEMFC

Reactions (Eqs. (1) and (2)) actually occur in several successive steps and can be affected by the presence of other reacting species. This section will thus focus on the main operating reactions together with the most impacting ones for the AL degradation.

2.2.1. Hydrogen adsorption and oxidation

Schuldiner et al. [48] have shown that, depending on potential range, a Pt electrode immersed in helium saturated 1 M H_2SO_4 solution was prone to oxygen or hydrogen adsorption and that these adsorptions were part of reactions (Eqs. (1) and (2)) mechanisms. They also measured an open-circuit potential (OCP) of +0.46 V vs. reference hydrogen electrode (RHE) when neither hydrogen nor oxygen atoms were adsorbed at Pt surface. Below this potential, reaction (1) proceeds in two successive steps, according to the mechanism firstly proposed by Heyrovsky and which is referred, as "the Volmer–Heyrovsky" mechanism [49]:

Adsorption of H atoms, at potentials ranging from +0.06 V to +0.13 V vs. RHE [48]:

$$H^+ + Pt + e^- \leftrightarrows Pt\cdots H \quad (4)$$

Hydrogen discharge step, between + 0.3 V and +0.46 V vs. RHE [48].

$$H^+ + Pt\cdots H + e^- \leftrightarrows H_2 + Pt \quad (5)$$

2.2.2. Oxygen reduction and adsorption on platinum

Several authors [48,50–53] have shown that, as soon as its potential raises above 0.8 V vs. RHE, the Pt surface is progressively covered by adsorbed oxygen species ($Pt\cdots O$). Thacker and Hoare [52] observed two types of adsorbed oxygen atoms, depending on potential (cf. Fig. 2). The "adsorbed oxygen", weakly adsorbed at metal surface, appears above +0.8 V vs. RHE and can reach 30% of a monolayer under open-circuit conditions. The so-called "dermasorbed oxygen" is absorbed in the first few atom layers of the metal at potentials higher than +1.0 V vs. RHE. Above +2 V vs. RHE, the $Pt\cdots O$ sites may even be converted to PtO_2 sites until a complete PtO_2 monolayer is formed. Under open-circuit conditions, PtO_2 sites decompose to $Pt\cdots O$ sites in the presence of bare Pt sites.

Damjanovic and Brusic [54] and Sepa et al. [55] elucidated O_2 reduction reaction (ORR) mechanism, which was summarized by Xu et al. [56]:

$$O_2 + Pt \leftrightarrow Pt\cdots O_2 \quad (6)$$

$$Pt\cdots O_2 + H^+ + e^- \leftrightarrow Pt\cdots O_2H \quad (7)$$

(rate-determining step)

$$Pt\cdots O_2H + Pt \leftrightarrow Pt\cdots OH + Pt\cdots O \quad (8)$$

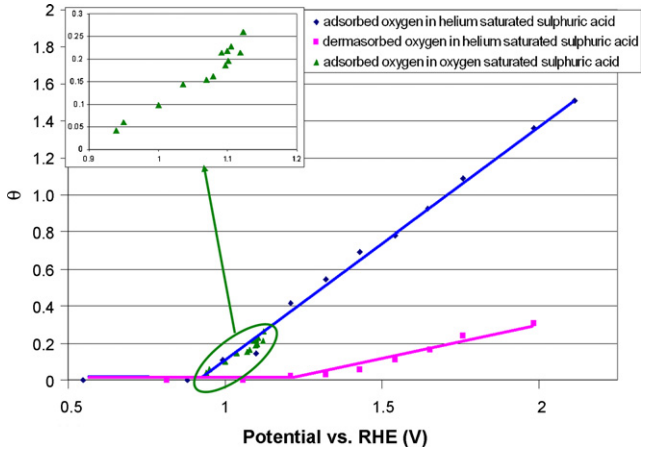

Fig. 2. Evolution with previously applied electrochemical potential of Pt surface coverage θ at OCV by adsorbed and dermasorbed oxygen, in oxygen and helium saturated 2N H_2SO_4. A full monolayer corresponds to $\theta = 1$. Replotted from Figs. 5 and 9 of ref. [52].

$$Pt\cdots O + H^+ + e^- \leftrightarrow Pt\cdots OH \quad (9)$$

$$Pt\cdots OH + H^+ + e^- \leftrightarrow H_2O + Pt \quad (10)$$

Xu et al. [56] also considered (Eqs. (10) and (9)) in the reverse direction as mechanism for platinum coverage with oxides.

2.2.3. Pt dissolution and reprecipitation

The Pt particles used in PEMFC have been proved to dissolve into Pt^{2+}, according to the following mechanism [57,58]:

$$Pt + H_2O \rightarrow PtO + 2H^+ + 2e^- \quad (11)$$

$$PtO + 2H^+ + 2e^- \leftrightarrow Pt^{2+} + H_2O \quad (12)$$

Eq. (11) is identical to the sum of Eqs. (10) and (9) in the reverse direction, except that a Pt oxide is considered instead of an adsorbed oxygen atom. It has standard equilibrium potential of +0.88 V vs. RHE [58]. If Pt^{2+} ions are more likely expected, some authors also detected Pt^{4+} [59–61].

Pourbaix diagram of $Pt^0/PtO/Pt^{2+}$ system at 25 °C [62] indicates that Pt metal can only be stable in the ionomeric phase for a negative pH and an electrochemical potential lower than approximately +0.9 V vs. RHE. Outside these conditions' domain, Pt^{2+} or PtO is more stable and Pt oxidation and/or corrosion is thermodynamically favored. However, equilibrium concentration in ionomeric phase remains very low: below 10^{-6} M and 10^{-9} M at potentials lower than +1.02 V vs. RHE and +0.92 V vs. RHE, respectively. Despite this, some authors [5,44,63] observed that platinum dissolves at potentials lower than those abovementioned: around +0.6–0.7 V vs. RHE. This can be explained by a higher operating temperature which thermodynamically favors Pt dissolution [5] or by the widely demonstrated Pt ion migration away from their original particle [5,12,21,24–26,44,64–68]. Indeed, this migration shifts the equilibrium of Eq. (12) in the dissolution direction, at a rate which increases with operating temperature.

In some cases, Pt ions migrate towards the neighboring particles and agglomerate with them especially in a wet operating medium, leading to an increase in particle average size. This mechanism is widely known as Oswald ripening [5,24,61] and its magnitude is increased when particle size is decreased, due to a greater thermodynamic driving force [61]. Dissolved Pt ions also migrate in the ionomer phase and in the polymer membrane that they contaminate [27,69,70]. Furthermore, once the Pt ions present in the ionomeric phase meet a reducing environment such as H_2 (stemmed from fuel crossover), they are reduced back into metallic Pt that precipitates in a solid Pt band either inside the membrane or at the cathode membrane interface [26,29,71]. Zhang et al. [64] and Bi et al. [26] showed that the Pt band position varies linearly with the ratio of hydrogen and oxygen partial pressures.

2.2.4. Carbon corrosion

Shao et al. [5] reported that the thermodynamic potential of carbon oxidation into CO_2 (Eq. (13)) is +0.207 V vs. RHE, which is lower than usual positive electrode potentials: carbon-support oxidation is therefore thermodynamically possible in the PEMFC standard operating conditions.

$$C + 2H_2O \rightarrow CO_2 + 4H^+ + 4e^- \quad (13)$$

Indeed, Roen et al. [72] observed CO_2 emission at carbon-supported Pt electrodes for temperatures lower than 50 °C. Baumgartner et al. [35] confirmed that, in a single cell operating at 70 °C at an applied current density of 0.4 A cm^{-2} with dead-end fuel supply and 2.2 overstoichiometric ratio of humidified air at 90%, CO_2 was produced at the cathode. Several authors [12,72,73] also observed that Pt accelerates carbon oxidation kinetics and that intermediate adsorbed CO specie is formed on the catalyst surface at potentials above +0.3 V vs. RHE. It is further oxidized to CO_2 at potentials between +0.6 V and +0.8 V vs. RHE. Finally, Ball et al. [66] showed that carbon corrosion occurs in three successive steps:

$$C \rightarrow C^+ + e^- \quad (14)$$

$$C^+ + H_2O \rightarrow CO + 2H^+ + e^- \quad (15)$$

$$CO + H_2O \rightarrow CO_2 + 2H^+ + 2e^- \quad (16)$$

It appears from the mechanism draw above that Eq. (15) might be a source of CO poisoning as observed by Roen et al. [72]. However, carbon corrosion rate at PEMFC's typical operating temperature (≈70 °C) is slow, even in the presence of catalyst and water. It increases with operating temperature and decreases with relative humidity [74]. It has also been shown that corrosion under load cycling to high cathode potentials (i.e. low current densities) are higher than during steady-state operation at the same potential levels [12].

2.3. Thermodynamics of PEMFC

The oxidation or reduction hierarchy of species present at an electrode surface depends on their respective equilibrium electrochemical potential values.

From a thermodynamic point of view, given specie can only be oxidized if it is the reducer of an electrochemical couple whose equilibrium potential is lower than the actual potential. Reversely, this compound can only be reduced if it is the oxidant of a couple whose equilibrium potential is higher than the actual potential. Similarly, when they are present simultaneously, an electrochemical couple's oxidant will spontaneously react with an other electrochemical couple's reducer as soon as the former couple equilibrium potential is higher than the latter's. This reaction can take place even without electronic transfer at the interface between electronic and ionic conductors, as a chemical oxido-reduction reaction.

The global reaction given in Eq. (3) is identical to the direct chemical reaction that occurs when both oxygen and hydrogen are directly in contact. From a thermodynamic point of view, path (a) in reaction (3) is spontaneous and characterized by a negative Gibbs free energy difference ($\Delta G_{(a)} < 0$). In addition, $\Delta G_{(a)}$ is independent from its chemical (gas mixture) or electrochemical (closed external electrical circuit) path and reaction will proceed until an equilibrium state is reached. At equilibrium, the reaction difference in Gibbs free energy will be zero and no further reaction occurs. $\Delta G_{(a)}$ is thus the maximum amount of energy that can be extracted from the H_2–H_2O–O_2 system, whatever its electrical or thermal nature [75]. According to Hamann et al. [75], the variation in free energy of half-reactions (Eqs. (1) and (2)) can be determined from their respective electrochemical potentials, according to Eqs. (17) and (18):

$$\Delta G_{(1)} = \Delta G^0_{(1)} + RT(2\ln a_{H^+,-} - \ln P_{H_2,-}) - 2FE_- \quad (17)$$

$$\Delta G_{(2)} = \Delta G^0_{(2)} + RT(2\ln P_{H_2O,+} - 4\ln a_{H^+,+} - \ln P_{O_2,+}) + 4FE_+ \quad (18)$$

Combination of Eqs. (17) and (18) gives, assuming that proton activity is constant in the whole volume of the MEA (due to the high dissociation of sulphonic acid groups in presence of water [56]) and the homogeneity of sulphonic acid group distribution within the MEA, the $\Delta G_{(a)}$ associated with overall reaction (3):

$$\Delta G_{(a)} = 2\Delta G_{(1)} + \Delta G_{(2)} = \Delta G^0_{(a)} + RT\left(\ln \frac{P^2_{H_2O,+}}{P^2_{H_2,-}P_{O_2,+}}\right) + 4F[E_+ - E_-] \quad (19)$$

The term inside the last brackets of Eq. (19) corresponds to the cell voltage U_{cell}.

At the equilibrium, since $\Delta G_{(a)} = 0$, we obtain:

$$\Delta G^0_{(a)} + RT\left(\ln\frac{P^2_{H_2O,+}}{P^2_{H_2,-}P_{O_2,+}}\right) = -4F[E_{eq,+} - E_{eq,-}] = -4FU_{eq} \quad (20)$$

This equation can also be rewritten in the form of Nernst equation:

$$OCV = U_{eq} = -\frac{\Delta G^0_{(a)}}{4F} - \frac{RT}{4F}\left(\ln\frac{P^2_{H_2O,+}}{P^2_{H_2,-}P_{O_2,+}}\right)$$

$$= \Delta E^0 + \frac{RT}{4F}\left(\ln\frac{P^2_{H_2,-}P_{O_2,+}}{P^2_{H_2O,+}}\right) \quad (21)$$

where OCV refers to the open-circuit voltage, i.e. the voltage at equilibrium (U_{eq}).

The combination of Eqs. (19) and (20) gives:

$$\Delta G_{(a)} = -4FU_{eq} + 4F[E_+ - E_-] = 4F[U_{cell} - U_{eq}] \quad (22)$$

This equation shows that reaction (3) can occur spontaneously (i.e. without external energy supply) only when $U_{cell} < U_{eq}$, which corresponds to path (a).

Electrochemical "reversible" systems can also operate in "electrolysis" mode but only in case of external energy supply. This corresponds to path (b) in reaction (3) for which $\Delta G_{(b)} > 0$ and $U_{cell} > U_{eq}$. Moreover, at the equilibrium, both $\Delta G_{(1)} = 0$ and $\Delta G_{(2)} = 0$. Therefore, both Eqs. (17) and (18) can also be rearranged as in the form of Nernst equations. For hydrogen electrode, Eq. (17) can be rewritten:

$$E_{eq,-} = -\frac{\Delta G^0_{(1)}}{2F} + \frac{RT}{2F}\ln\frac{a_{H^+,-}}{P_{H_2,-}} = E^0_- + \frac{RT}{2F}\ln\frac{a_{H^+,-}}{P_{H_2,-}} \quad (23)$$

2.4. Kinetic considerations

2.4.1. Overview of electrochemical kinetics

In electrochemical cells like fuel cells, reactions imply charge transfers between electrons conducting materials and reactant species. In addition, reactant gases need to diffuse from supply channels to the sites where electrochemical reactions take place. However, these electron and reactant transfers are not instantaneous and the corresponding kinetic limitations induce voltage losses, respectively known as activation (or charge transfer) and concentration (or mass transfer) polarizations. The total kinetic polarization is given by Butler–Volmer equation that can be written as follows for a given electrode [49,75–77].

$$j = j_{eq}\left[\frac{j_{lim,Red} - j}{j_{lim,Red}}.e^{(\alpha\nu_e F/RT)(E-E_{eq})} - \frac{j_{lim,Ox} - j}{j_{lim,Ox}}.e^{-((1-\alpha)\nu_e F/RT)(E-E_{eq})}\right] \quad (24)$$

where j_{lim} is the limiting current density, i.e. the maximum current density that can be applied for a given reaction. In absence of mass transfer limitations and far from equilibrium, the Butler–Volmer equation can be approximated by Tafel equation:

$$E - E_{eq} = \eta = \frac{RT}{\alpha\nu_e F}\ln\frac{j}{j_{eq}} \quad (25)$$

In addition to these polarization losses, there are also ohmic losses associated with charge transfer inside the conductive materials (mostly the ionomer for fuel cells). Their increase is related to several mechanisms like membrane drying [6,17,78–82], membrane contamination [15,18], high contact resistance between cell elements, thermal degradation.

In a generator like a fuel cell, all polarizations and ohmic losses are subtracting from the OCV since, as explained in Section 2.3, the maximum amount of energy that can be extracted from the system is defined by the reaction's difference in Gibbs energy. Therefore, we have [43,49,83,84]:

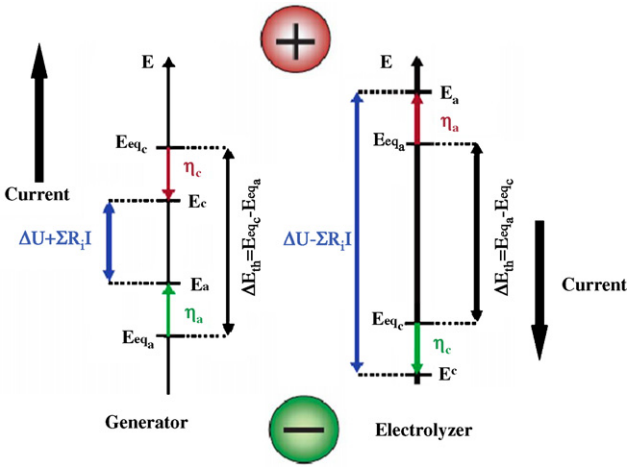

Fig. 3. Contribution of ohmic drop and both anodic and cathodic polarizations to the potential difference in an electrolyzer or a generator [84].

$$U = (E_{eq,c} - E_{eq,a}) - \eta_a - |\eta_c| - ir \quad (26)$$

Oppositely, as explained in Section 2.3, when an electrochemical cell operates in "electrolysis" mode, the reaction is not spontaneous and energy has to be provided to the system with a minimum amount, corresponding to reaction's difference in Gibbs energy. Therefore, all ohmic drops and polarizations have to be overcome and additional voltage has to be supplied to the OCV to perform the reaction. Therefore [49,84]:

$$U = (E_{eq,a} - E_{eq,c}) + \eta_a + |\eta_c| + ir \quad (27)$$

In addition, it is worth pointing out that, as shown in Fig. 3, in the case of a "reversible" system (i.e. that can operate in both generator and electrolysis modes), the polarities of anode and cathode electrodes are reversed. This is due to the reverse direction in which reactions occur and to the convention that reduction reactions take place at the cathode and oxidation reactions take place at the anode [75,84]. That is why we will mostly talk about "positive" and "negative" electrodes in this document.

2.4.2. Kinetics of oxygen reactions at Pt electrodes

In a fuel cell, the oxygen reduction reaction (ORR) was shown to be three orders of magnitude slower than the hydrogen oxidation reaction (HOR) [85] and cathodic activation polarization represents the major part of voltage losses. That is why this reaction has drawn a lot of research effort for many decades.

Damjanovic et al. [50] first demonstrated that the kinetics of the ORR on a bare Pt electrode immersed in 2 M sulphuric acid significantly depends on whether the electrode surface is covered with oxide or is oxide-free. This result was further confirmed by Zecevic et al. [86] on Pt covered with thin Nafion film or polybenzimidazole (PBI) solid polymer electrolytes. Several authors showed, either for bare Pt electrodes in sulphuric acid solutions of different pH [53–55,87,88] or at Pt–Nafion interface [86,89–94], that ORR's current voltage curves exhibit two different Tafel slopes with a smooth transition between them (Fig. 4). At Pt microelectrode–Nafion interface, this behavior was observed for various oxygen partial pressure between 0.078 and 7 atm [92] and different temperatures between 30 and 80 °C. The first slope, at low current densities (i.e. potentials above +0.8 V vs. RHE), is $-RT/F$, while the second slope, at high current densities, is $-2RT/F$.

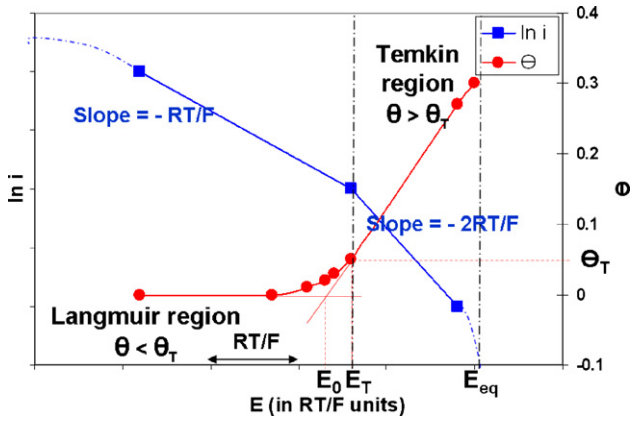

Fig. 4. Influence of Pt electrode potential on ORR current density (curve with squares) and on oxide surface coverage θ (curve with circles). Replotted from Figs. 1 and 2 of ref. [88].

In both regions, Sepa et al. [55,88] showed that the rate-determining step (RDS) at a Pt/liquid acid interface was identical and corresponded to Eq. (7), in accordance with results of Damjanovic and Brusic [54]. Zecevic et al. [86] further demonstrated that ORR kinetics on Pt covered with thin film of either Nafion or PBI and immersed in liquid acid were not altered by the recast polymer and generalized the results to PEMFC operating conditions. Antoine et al. [89] estimated, for Pt nanoparticles dispersed in Nafion ionomer, the exchange current densities at around 10^{-10} and 10^{-7} A cm^{-2}, respectively for the low and high current densities regions. The different Tafel slopes were shown to arise solely from different adsorption conditions of reaction intermediates [55,86,88]. At low current densities, oxide coverage is high and interferes with ORR kinetics: Temkin adsorption conditions prevail, i.e. surface concentration of adsorbed species varies linearly with potential. At high current densities, oxide coverage is very low and Langmuir adsorption conditions prevail. The transition comes at a potential E_T, corresponding to a surface coverage of $\theta_T \sim 0.05$ [88]. This potential increases with temperature while the corresponding current density decreases [93] but carbon support or Pt particle size has little influence on ORR kinetics parameters [94].

However, Parthasarathy et al. [93] suggested that, in the lower current density region, the rate-determining step could be the chemical step which follows directly the first electron transfer step (Eq. (7)). This chemical step was suspected by Xu et al. [56] to be the O–O bond cleavage (Eq. (8)). They indeed explained that first electron transfer could be fast in PEMFC due to the high surface areas of Pt/C electrodes and to the high proton activities in Nafion ionomer, above all when operating at high relative humidities (RH). Moreover, O–O bond cleavage needs two adjacent Pt sites to proceed, which could be difficult in case of high oxide surface coverage. At low RH, however, reaction (7) could be rate determining due to lower surface coverage and lower proton activity. This RH effect was explained by reaction (10). High RH should indeed favor the adsorption of oxygenated species by facilitating Pt oxide surface coverage, which could in turn affect the ORR. Indeed, –OH and –O adsorbed on the Pt active sites block the oxygen molecules from reaching the surface and prevent O–O bond from further splitting after the adsorption of $-O_2H$.

2.5. Considerations about mixed potentials

In standard conditions, a fuel cell's OCV value should be +1.23 V, but under practical conditions, a typical PEM fuel cell's OCV is below +1 V [95].

As explained in Section 2.3, the oxidant from an electrochemical couple will spontaneously react with the reducer of another electrochemical couple if the former couple's equilibrium potential is higher than the latter's. However, these oxido-reduction reactions are often kinetically slow and the two half-cell electrode potentials might coexist separately on a same electrically conductive surface. Since the surface is an electronic conductor and therefore is equipotential, it is somehow in short-circuit and a local current i_{mix} will flow. The electrode potential will then be a "mixed potential" and its actual value will be between both reactions equilibrium potentials, at a value which will depend on the relative polarization of both reactions. The mixed potential can be determined by Evans diagrams [96].

Such mixed potential is widely known in corrosion field [96] but has also been proved to be at the origin of the significant difference between the actual and theoretical OCV in both PEMFC [52,53,55,56,58,88–94,97] and DMFC [98–100]. In the case of PEMFC, the most widely involved couples are: O_2/H_2O on the one hand and PtO/Pt^0 (oxide film formation) [55,56,58,88–94,97], Pt^{2+}/Pt^0 (Pt dissolution) [55] and/or either carbon-support material [56], permeated hydrogen [56] or organic impurities oxidation [53,91,94,97] on the other hand.

However, Sepa et al. [55] showed that Pt dissolution reaction was the major anodic component for the mixed potential and summarized their analysis in an Evans diagram presented in Fig. 5. They estimated the mixed current density i_{mix} at about 10^{-6} A cm^{-2}. For comparison, Parthasarathy et al. [90] determined by impedance spectroscopy respective i_{mix} values of 4.4×10^{-7} A cm^{-2} and 1.6×10^{-5} A cm^{-2} in the low and high current density regions at a Pt–Nafion interface. They also showed that by increasing temperature, the mixed potential was shifted closer to the reversible oxygen electrode potential due to the higher rate of ORR.

Interestingly, many studies dealing with development of hydrogen sensors based on proton conducting media and Pt electrodes were performed in operating conditions close to those prevailing in case of fuel starvation or H_2 crossover (i.e. low amount of H_2 in O_2 or air). These studies have demonstrated that a mixed potential between H_2/H^+ and O_2/H_2O was established on the sensors' electrode [101–106], whatever its morphology. The basic principle of these sensors was first described by Miura et al. [103] but Opekar [104] was the first to use a Nafion membrane coated on both sides with Pt which serves as solid polymer electrolyte and proton supply for the cell reaction.

Opekar et al. [105] first observed that the evolution of Pt electrodes' steady-state potential with hydrogen partial pressure exhibits two different behaviors. Bouchet et al. [101,102] further studied over a wide range the influence of hydrogen partial pressure in air or inert gases on the OCP of E-TEK PEMFC gas diffusion elec-

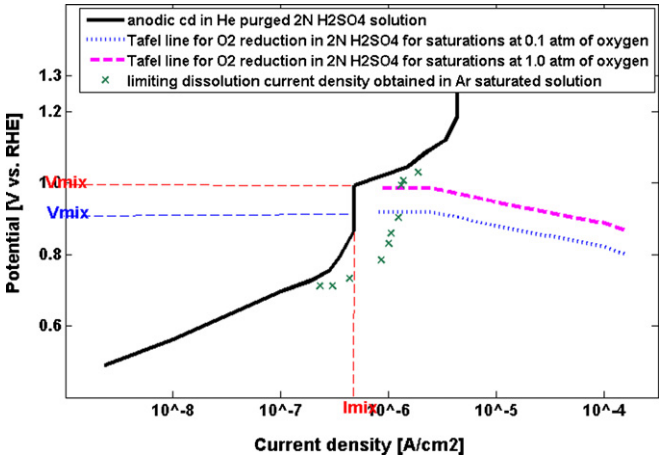

Fig. 5. Evans diagram of Pt dissolution and O_2 reduction reactions [55].

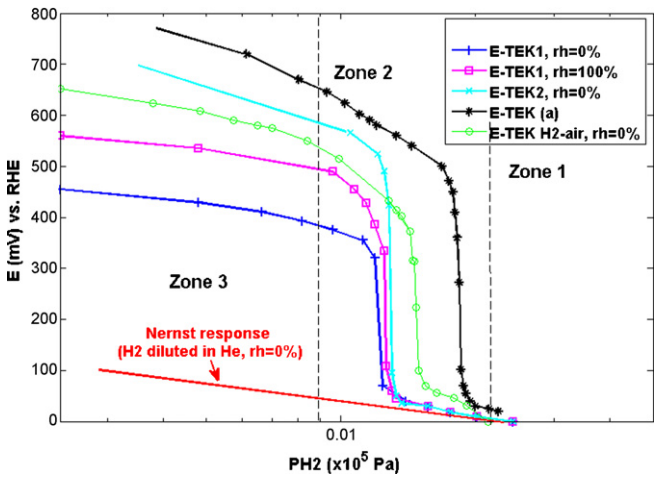

Fig. 6. Evolution of different E-TEK gas diffusion electrode OCP with hydrogen partial pressure in different atmospheres. Replotted from Figs. 5 and 9 of ref. [102] and Figs. 3 and 4(a) of ref. [101].

trode using PBI as proton conducting media instead of Nafion. They checked that PBI does not influence the ORR mechanism by comparing their results with those obtained by Vermeijlen and Janssen [107] and observed a sigmoidal dependence of OCP vs. H_2 partial pressure, with three main regions (cf. Fig. 6):

- for high H_2 partial pressure (region 1), O_2 partial pressure is negligible so that the electrode's OCP is fixed by H_2 oxidation and follows Nernst equation (23), whatever the Pt electrode type (grid, film or small particles dispersed on carbon in E-TEK gas diffusion electrode).
- in region 2, OCP evolution exhibits a sharp transition. Oxygen and hydrogen concentrations at the electrode are low, resulting in mass transfer limitations of both hydrogen oxidation and oxygen reduction reactions. A transition from a hydrogen electrode to an oxygen electrode occurs, resulting in the OCP's very high sensitivity. The H_2 pressure range where this sharp variation takes place and its shape highly depends on Pt electrode morphology [102] but is independent of Pt loading [106]. Rosini et al. [106] also showed, by numerical simulation, that decreasing the ratio between actual and geometrical surface areas, increasing the active layer thickness or decreasing the oxygen diffusion rate induce a decrease in the abruptness of the potential change and a broadening of the region where the potential change takes place.
- in region 3, the hydrogen concentration at the electrode becomes very low and the electrode rather acts as an oxygen electrode. Therefore, its potential evolution with hydrogen partial pressure exhibits two linear segments with respective slopes of $-RT/F$ and $-2RT/F$, corresponding to the Tafel slopes determined for oxygen reduction at all Pt electrodes in either acidic media or impregnated with Nafion [53–55,87–94].

3. Long-term catalyst and carbon-support degradations

During long-term ageing at normal operating conditions, fuel cell voltage only "reasonably" decreases. This decrease is due to the harsh conditions in which fuel cell medium is exposed. Metallic catalyst and carbon-support degradation rates are accelerated by different operational conditions and parameter levels: cathode electrochemical potentials above 0.6 V vs. RHE [74,108], very low pH (due to MEA highly acidic environment [60,108]), high humidity [74,109–111] and operating temperature [109,110].

One of the main observed degradation associated with long-term ageing is a continuous decrease of electrochemically active catalyst surface area mainly associated with Pt dissolution, migration and reprecipitation [21–23,27,59,74,112,113] (as explained in Section 2.2.3). Indeed, Wilson et al. [25] and Murthy and Sisofo [108] reported, after 2000 h of continuous operation at 80 °C, catalyst active area losses at PEMFC cathode of 60% and 80% at 0.5 V and open-circuit voltage, respectively. Pt loss also arises from carbon corrosion [44] that releases the no more supported particles. According to Guilminot et al. [59], carbon corrosion can result in a cathode thickness decrease up to 60%. This electrochemical surface area (ESA) decrease increases in turn the activation overpotential by increasing the actual current density at catalyst level.

In addition to the effects observed in steady-state conditions, the rate of long-term degradation strongly depends on power and thermal cycling [74,109,114–119]. Such cycling is inherent to many applications. Mathias et al. [70] reported that a vehicle experiences about 300,000 voltage cycles between peak power (+0.7 V vs. RHE) and idle (+0.9 V vs. RHE) through a life of 5500 h. Several studies comparing the long-term performance of hydrogen–air PEM fuel cells aged under cyclic loading conditions and under constant load mode [5,45,70,74,111,115–117,120] showed that catalyst degradation rate is "accelerated" by cycling. Roen et al. [72] indeed showed that the loss of Pt surface area increases with the number of cycles, the potential cycling level and the time spent at it. This was explained by the fast hydrogen oxidation kinetics that ensures a high stability of the negative electrode potential which remains almost constant and close to the reversible hydrogen potential [70]. As a consequence, the positive electrode will carry almost all the changes in applied power and the cathode potential might reach high potential values [121]. In addition, Harel et al. [115] and Wahdame et al. [116] showed that, under cycling mode, both the average current value and flow strategy adopted over the cycle have a great impact on the degradation rate.

Finally, Cho et al. [109] thermally cycled between 80 °C and −10 °C a single cell potentiostated at 0.6 V vs. RHE and observed a degradation rate of −2.8% per cycle of the output current at 80 °C while the OCV remained constant (V_{OCV} = 1.0 V vs. RHE). This degradation was mainly attributed to ohmic and activation losses increase resulting from catalyst layer mechanical "deformation".

4. Starvation

In this paper, starvation will refer either to local undersupply of reactants associated with uneven distribution while overall supply at cell level is sufficient [11,29–31,33,36,122–124] or to an overall undersupply of reactants at cell level [8,37,39]. The former will be called "local starvation" while the latter will be called "overall starvation". All fuel cells are potentially subject to these dangerous operating conditions, which can affect one or several cell in a stack. Moreover, starvation can occur either at positive electrode or at negative electrode but fuel starvation was proved to be more harmful to the cell than oxidant starvation [9,32,38,40], thus driving a lot of research efforts in the past decades.

4.1. Causes and consequences of starvation

Several causes of starvation have been reported in the literature [4,8,9,31,33,35–40,123]:

Improper gas supply: Flow-field channels obstruction by liquid water [33,35] or ice [11,29,33,35] and fuel cell design anomaly can both induce uneven gas distribution or even local insufficient supply of reactants (depleted gases). Improper gas supply could for instance be a consequence of the presence of nitrogen molecules at the electrode. Coming from air fed in the fuel cell's cathodic com-

partment, nitrogen molecules could accumulate during operation [29,125,126] and further migrate, due to the concentration gradient, towards the anode where they accumulate near the gas exit. They further impede the fuel to reach the AL which causes local starvation. Another cause of improper gas supply could be a low reactant flow rate aiming at maximizing reactant utilization in order to optimize fuel cell efficiency. Unfortunately, low flow rates may induce uneven flow sharing between the cells in a stack, leading to locally or completely starved cells. [39].

Sudden load increase: after a sudden load demand, the reactant feeding might not follow fast enough the current increase, leading to transient starvation.

Start-ups [11,30,31,33,122,124]: In addition to the problem associated with sudden load increase, start-ups might be affected by the possible presence of air inside the anodic compartment, particularly after a prolonged shut-down [33]. Indeed, despite the efforts made to improve stacks' sealing towards the ambient air, hydrogen leaks out due to the gradient in partial pressures between compartments and the ambient air, and is progressively replaced by it. In addition, oxidant crossover to the anode [33,121] occurs. At start-up, the anode is fed with fuel and this fuel displaces the air, creating a fuel-air front along the anode catalyst layer and causing transient localized or even complete fuel starvation [11,30,31,33,121,122,124]. Similarly, after a shut-down followed by a nitrogen purge, an oxidant starvation could occur by the formation of a nitrogen–air front.

The main consequences of fuel cell starvation are catalyst loss and carbon-support corrosion. Taniguchi et al. [8] observed that the decrease of cathodic active area in a starved cell is associated with an increase in the mean size of catalyst particles, and the disappearing of smallest particles. Active surface area loss is evaluated by electrochemical measurements (cyclic voltammetry) while the particles size and the uniformity of their dispersion are observed by TEM analysis and X Ray Diffraction [61,74]). In addition, corrosion rates are calculated from CO_2 and CO concentration in the cathode exhaust, which are measured by non-dispersive infrared spectroscopy (NDIR).

4.2. Fuel starvation

4.2.1. Local fuel starvation

4.2.1.1. Starvation associated with improper gas supply. In normal operating conditions, when reactants are sufficiently supplied and evenly distributed at the electrode surface, the current distribution is homogeneous and so are all polarizations and ohmic losses. Nevertheless, in case of heterogeneous reactant gas distribution, polarization losses increase in the areas of lower reactant concentrations through its mass transfer component. As a consequence, current tends to flow in the areas of higher reactant partial pressure so as to limit mass transfer losses, creating a heterogeneous current distribution [127]. This heterogeneous distribution has been clearly evidenced by several authors [37,39], who studied the influence of operating conditions on current distribution, in a segmented single-cell. Except Liu et al. [138], they all operated at fixed cell potential guarantees that no overall starvation is possible: current output is indeed intrinsically limited. Current density distribution is affected by operating conditions such as: stoichiometries of reactant gases, humidification conditions, microstructure of the gas diffusion electrode (thickness, structure, ionic and electronic conductivity, gas diffusion layer) and flow field design [138]. Natarajan et al. [37] thus showed that, in case of excess hydrogen supply (overstoichiometric ratio of 2), the current distribution was homogeneous (Fig. 7). However, as the applied voltage was decreased, fuel utilization increased to a hydrogen overstoichiometric ratio of 1.25 and the current flew only on the four segments located nearest to the fuel inlet while almost no current flew in the segment located at gas outlet. With a further increase in applied voltage,

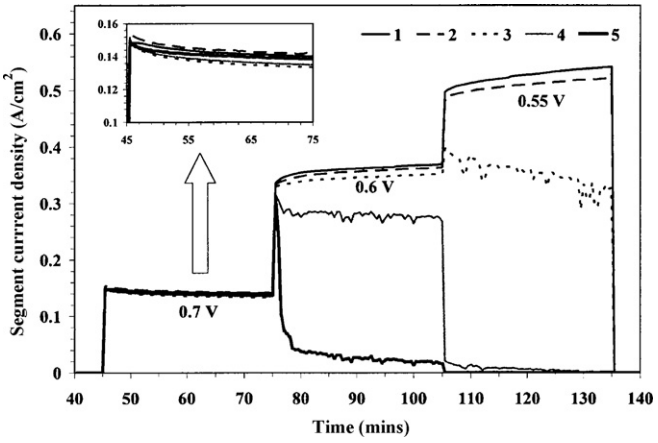

Fig. 7. Individual segment current response at various applied voltages, corresponding to different hydrogen overstiochiometric ratios. Inset provides an enlargement at 0.7 V applied voltage. Respective H_2 and O_2 flow rates equivalent to 0.28 A cm^{-2}, and 1.05 A cm^{-2} [37].

fuel utilization tended towards 1 and an even more heterogeneous current distribution was observed, with an absence of current in the two segments located near the gases outlet. The gas inlet relative humidities did not change significantly the applied potential effect on current distribution, only a small resistivity effect due to lower membrane water content was observed at low current densities (high applied voltages) [37]. This indicates a predominant reactant mass transfer limitation effect. Liu et al. [39] confirmed these results by plotting each segment's polarization curves in potentiostatic mode): as soon as the applied voltage decreased below 0.7 V vs. RHE, the current distribution became heterogeneous and even completely fell down for segments located at gas outlet. Sun et al. [139,140] and Hottinen et al. [141] also showed that, when the cell is highly under-humidified, the local current density increases monotonously along the channel due to progressive membrane hydration by produced water that increases membrane ionic conductivity. When the cell is well-hydrated or over-hydrated, the local current density decreases monotonically along the channel due to both reactant partial pressure reduction (which in turn increases in the mass transfer overvoltage) and cell flooding in the downstream part (which prevents reactant gases to reach active sites). In an intermediate range, local current density first increases, reach a maximum, and then decreases along the channel due to the abovementioned opposite effects. [139–141].

Baumgartner et al. [35] followed the evolution of membrane electrochemical potential at 4 different locations in the fuel channel while the cell was operated at a 2.2 overstoechiometric ratio for oxygen in air humidified at 90%, and either in dead-end mode or in overstoechiometric ratio decreasing from 1.5 to 0.95 for dry hydrogen supply. The applied current density was fixed at 0.4 A cm^{-2} and the temperature at 70 °C. Their results are summarized in Fig. 8 for the dead-end mode experiments. Similar trends and curves shape were obtained when they decreased the hydrogen stoechiometric ratio from 1.5 to 1. According to their experimental description, anode and cathode potentials respectively correspond in to $E_{eq,a} + \eta_a$, which corresponds to the potential drop at negative electrode/membrane interface, and $E_{eq,c} - |\eta_c| - ir$. As explained by the authors, just after a purge (between 500 and 600 s in Fig. 8(a)) or for high hydrogen overstoechiometric ratios, current distribution is homogeneous and the potential drop at negative electrode/membrane interface is almost uniform. Moreover, cell voltage is close to $E_{eq,c} - |\eta_c| - ir$. Nevertheless, either in dead-end mode or for hydrogen overstoechiometric ratios slightly higher than 1, a gradient in hydrogen partial pressure is progressively created and increases in magnitude as operation proceeds. Meanwhile,

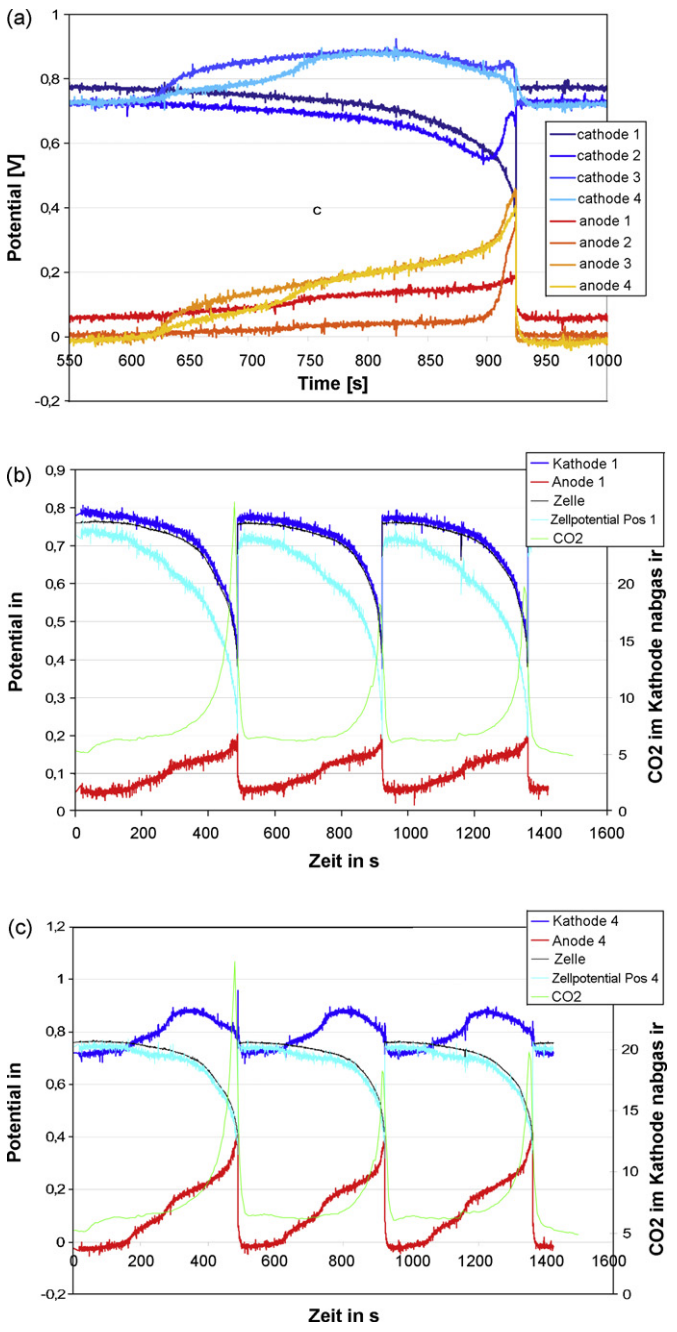

Fig. 8. (a) Measurement points 1–4 corresponding to different segmented regions in the cell. (b, c) Comparison of electrode potentials at positions 1–4 during dead-end operation [31].

in dead-end mode, nitrogen and water accumulates in the anodic flow field end, accentuating the gradient. As soon as hydrogen partial pressure has significantly decreased in the regions far from gas inlet, as shown in Fig. 8(a) to (c), the corresponding local negative electrode potential increases due to an increase of both HOR overvoltage and H^+/H_2 Nernst potential. Therefore, a gradient in the voltage drop at negative electrode/membrane interface is created. To ensure a homogeneous electrical potential in the electronic conductive material, the current redistributes with a higher local density in regions of lower resistance, i.e. at hydrogen supply end. This redistribution impacts the positive electrode where the ORR overvoltage and the ohmic drop are locally decreased. This simultaneously induces an increase of $E_{eq,c} - |\eta_c| - ir$ value in regions located near the dead end (Fig. 8(c)) and therefore exposes the cathode to higher electrochemical potentials. The higher electrochemical potentials favor both Pt dissolution and carbon corrosion (Fig. 8(b) and (c)), as explained in Sections 2.2.3 and 2.2.4. The $E_{eq,c} - |\eta_c| - ir$ value drops in regions located near the fuel supply where current progressively concentrates, locally increasing cathodic overvoltage and ohmic drops.

In parallel, except at hydrogen inlet, when the regions near the gas outlet are strongly depleted in hydrogen, the potential drop at negative electrode/membrane interface rises sharply. For operation in low and constant overstoechiometric ratios and on the basis of the model presented by Reiser et al. [121] (see next section), the authors explained this behavior by oxygen permeation through the membrane and by possible local electrolysis. At first sight, their analysis was confirmed by a cell reversal when they decreased the hydrogen overstoechiometric ratio from 1 to 0.95, that was associated with an hydrogen release at the cathode and a high increase in CO_2 release at the anode which also exhibited a potential of +1.5 V vs. RHE, indicating that the cell operated at least partly in electrolysis mode.

However, at single cell level, this analysis seems in deep contradiction with thermodynamics which, as explained in Section 2.3, tells us that a reaction, whatever its chemical or electrochemical nature, can only be spontaneous if its variation in Gibbs free energy is negative. And this condition is valid only when operating in fuel cell mode (i.e. without cell reversal). When operating in electrolysis mode, difference in Gibb's free energy is positive and external energy has to be supplied to the system to overcome OCV and all polarizations and ohmic drops. If, at stack level, such energy can undoubtfully be provided by the cells located in the upstream current flow, this energy source has to be found at single cell level. In the case of Baumgartner et al. [35], a close look at their experimental description shows that they used a Zahner IM6ex potentiostat, which can operate both as an energy source or an energy sink [128]. This equipment therefore allowed them to correctly simulate what happens in a stack containing some reversed cells but does not appear to be representative of phenomena occurring at single cell level. As far as we are concerned, based on all results summarized in Section 2.5, an alternative interpretation can be proposed, on the basis of a mixed potential associated with oxygen permeation, to explain the behaviors observed at single cell level. Indeed, the evolutions with hydrogen partial pressure of E-TEK Pt electrodes potential in a hydrogen–air mixture presented in Fig. 6 are very similar to the evolution of $E_{eq,a} + \eta_a$ presented in Fig. 8. This suggests us that $E_{eq,a}$ is actually a mixed potential between the equilibrium potential of a Pt electrode in contact with pure and highly concentrated hydrogen (which actually prevails when fuel cell operates in "normal mode") on the one hand, and the one that would prevail at a Pt electrode in contact with a gas mixture of hydrogen strongly diluted in oxygen and nitrogen (which would follow the trend shown in Fig. 6), on the other hand.

4.2.1.2. Starvation associated with start-up. When a fuel cell is shutdown, ambient air may introduce in the gas channels where it replaces hydrogen. During start-up, a transient fuel–air front is created along the anode catalyst layer that may cause localized or even complete fuel starvation. This further induces rapid carbon corrosion, resulting in dramatic catalyst active area and fuel cell performance losses. Therefore, a lot of work has been done to understand what occurs during start-up [11,29–31,108,122,124].

Reiser et al. [123] first modeled the degradation occurring during start-up in order to define the conditions that favor cathode carbon oxidation and determine the profile of electrode/electrolyte potential drops in presence of a fuel–air front at the anode. Meyers and Darling [29] also simulated the effects of a maldistribution of hydrogen at the anode in both steady-state and transient operation. As shown in Fig. 9, both models assumed that hydrogen oxidation

reaction occurs normally in the region filled with fuel while, in the fuel-starved region, oxygen reduction occurs at the anode and carbon corrosion as well as oxygen evolution occur at the cathode. These authors assumed that, thanks to the highly conductive bipolar plates and the low membrane thickness, the two electrically connected regions are coupled by electron transfer while no proton transfer could occur. They thus concluded that the anode metal potential is equal to hydrogen reduction reaction's potential. Their models also predict that the electrochemical potential of anodic regions filled with oxygen equilibrates to the oxygen potential which may create locally favorable reverse-current conditions in these exposed regions. The created reverse-current causes local cathode catalyst degradation due the cathode high interfacial potential that was calculated at 1.44 V vs. RHE [121] or even 2 V vs. RHE [29]. The authors called this mechanism "the reverse current decay mechanism".

However, according to the description given by Reiser et al. [121], their model relies on the hypothesis that the potential drop at electrode/membrane interface is different in air and hydrogen filled regions and that they respectively correspond to equilibrium potentials of Eqs. (1) and (2). Nevertheless, this hypothesis might be questionable since, as explained in Section 2.5, it is widely demonstrated, including in the case of air and hydrogen mixtures of various compositions in contact with Pt electrodes [101–106], that when two reactions involving two different electrochemical couples occur simultaneously in two opposite directions at the same electrode, a mixed potential is established at this electrode/solution interface, which magnitude relies between both couples' electrochemical potentials.

In order to validate their model, Reiser et al. [121] first used a single cell with two separated gas flows at the anode: one for hydrogen and one for either nitrogen or diluted oxygen. In all experiments, cathode was fed with air. They observed that the cathode area facing the anodic part fed with either nitrogen or diluted oxygen exhibited very strong thickness decrease, while the remaining part was not affected. In case of feeding with nitrogen, oxygen was supposed to permeate from cathode to anode. The authors thus concluded that these results validated the "reverse current decay mechanism". However, they did not measure the high cathodic potentials expected from their model and, as explained in Section 4.2.1.1, the observed degradations at the cathode could also be explained by heterogeneities in current distribution with local current close to zero in the area fed with nitrogen or diluted oxygen. This very low actual current further induces local cathodic potential drops closed to the equilibrium potential which, as described in Sections 2.2.3 and 2.2.4, can in turn explain the degradations [97].

Reiser et al. [121] also used two single O_2/H_2 and air/air cells connected together electrically, as shown in Fig. 10. Assuming that proton conductivity was very low in the plane direction, they considered this setup as representative of Fig. 9's cell configuration, where the electric leads play the role of bipolar plates. The cells were held at OCV for 1 h in room temperature and then 2 h at 65 °C. After each time intervals of 1 h, Cell 2 exhibited significant performance losses, associated with 4%, 25% and 50% reduction of electrochemical active surface area (ECSA). Once again, Reiser et al. [121] attributed these degradation to the "reverse current decay mechanism". They indeed explained that, in this set-up and as predicted by their model, Cell 2's anode was fed with the electrons produced at Cell 1's anode and that Cell 1's cathode was fed with electrons coming from the Cell 2's cathode. As a consequence, they considered that oxygen reduction reaction potentially occurs at Cell 2's anode and that either oxygen evolution or carbon corrosion potentially occurs at its cathode. However, in this configuration, since these two cells are neither connected to an electronic load or a potentiostat and since they are only externally connected, the set-up presented in Fig. 10 most likely represent a generator (Cell 1) connected in series to an electrolysis cell (Cell 2) rather than two single fuel cells connected in parallel. Therefore, according to Kirchhoff's voltage law:

$$U_1 = U_2 + ir_{\text{wiring}} \tag{28}$$

where r_{wiring} stand for ohmic resistances in connecting wires.

In this case, Cell 1, which is fed by hydrogen and air, provides energy through a current that can be calculated by combining equations (22) and (26):

$$i = \frac{(U_1 - U_{1,\text{eq}}) - \eta_{1,\text{a}} - |\eta_{1,\text{c}}|}{r_1} = \frac{-(\Delta G/4F) - (\eta_{1,\text{a}} + |\eta_{1,\text{c}}|)}{r_1} \tag{29}$$

This current further makes Cell 2, which is fed with air in both compartments and therefore can not provide any significant energy, operate in electrolysis mode. Cell 2's voltage can further be calculated by combining Eqs. (27) and (29), as follows:

$$U_2 = U_{2,\text{eq}} + \eta_{2,\text{a}} + \eta_{2,\text{c}} + \frac{-(\Delta G/4F) - (\eta_{1,\text{a}} + |\eta_{1,\text{c}}|)}{r_1} r_2 \tag{30}$$

Therefore, as shown in Fig. 11, Cell 2's positive electrode can reach high enough potentials for fast carbon and Pt corrosion to occur.

Tang et al. [11] also aimed at validating the "reverse current decay mechanism" and adopted the same experimental set-up as Reiser et al. [121], except that, in addition to the electrical connection between each cell's positive and negative electrodes, they also physically connected both cells' gas channels: Cell 1's negative and positive electrode compartments' exhausts are respectively connected to Cell 2's negative and positive electrodes compartments' inlet (cf. Fig. 12(a)). Air was continuously fed to the positive compartments while air and reformate were alternatively and repeatedly fed to the negative compartments by switching on and off their respective manifolds. Fig. 12(b) presents the evolution during one cycle of Cell 1's voltage and current flowing from Cell 1's to Cell 2's negative electrodes.

Prior to any gas switch, no physical or electrical connection was done and both positive compartments were filled with air while

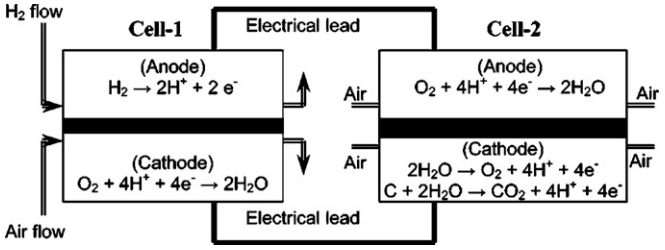

Fig. 10. Configuration of the two cells in the experiment of Reiser et al. [121].

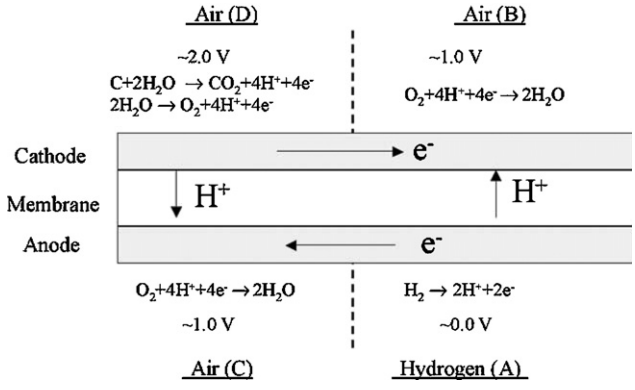

Fig. 9. Illustration of Reiser et al.'s model of reverse current mechanism [11,121].

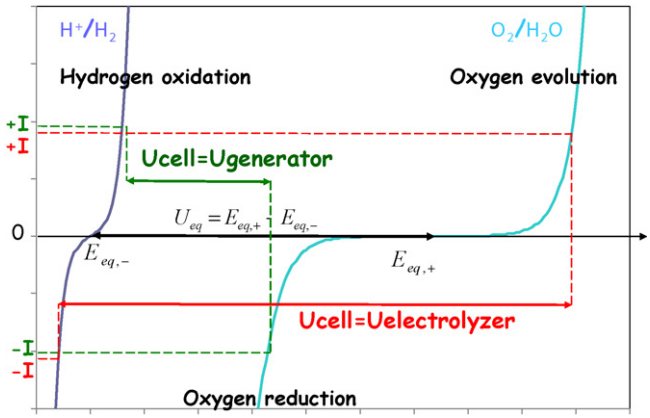

Fig. 11. Intensity potential curves for two electrodes of an electrochemical cell.

Cell 1 and Cell 2's negative compartments were respectively filled with reformate and air. Then, Cell 1 and Cell 2 exhibited respective voltages of 0.93 V and 0 V. Once electrically connected, Cell 2's voltage rose immediately to 0.82 V. Therefore, Tang et al. [11] assumed that, since Cell 2's negative electrode was fed with air, its potential vs. Cell 1's negative electrode potential should be around 0.93 V and deduced that Cell 2's positive electrode potential was around 1.75 V (vs. Cell 1's negative electrode potential). They thus concluded that the electrochemical potential reached by Cell 2's positive electrode was compliant with the "reverse current decay mechanism". However, like in the experiment of Reiser et al. [121], both cells are neither connected to an electronic load nor to a potentiostat but only externally connected via a multimeter and, therefore, the same analysis can be made. Indeed, the authors observed a current flowing from Cell 2's negative electrode to Cell 1's negative electrode, i.e. from Cell 1's (the generator) positive electrode to Cell 2's (the electrolyzer) positive electrode (cf. Fig. 12(b), just before the mention of "air entering in Cell 1"). Tang et al. [11] then switched the negative compartment's flow from reformate to air (beginning of Case 1 in Fig. 12(b)). Despite the mention in Fig. 12(b) that reformate only started to enter Cell 2 once Cell 1 was completely filled with air, it seems more likely that reformate is progressively pushed away from Cell 1 into Cell 2 by the air fed in Cell 1, and that it is further pushed out from Cell 2 as air enters it. In addition, air and reformate might mix and part of the reformate is likely consumed by measured current production. Once Cell 2 was completely filled with air, reformate is fed again in Cell 1's negative compartment.

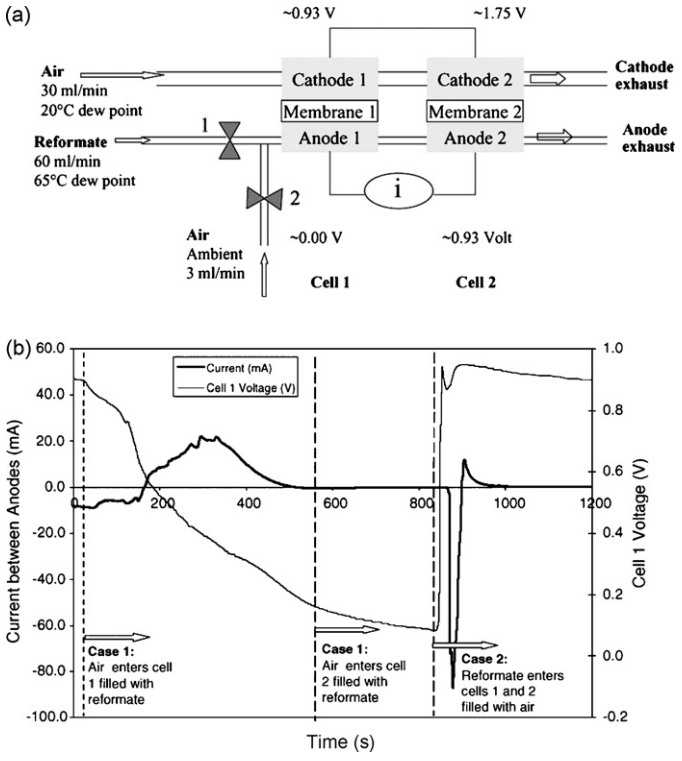

Fig. 12. (a) Experimental setup used by Tang et al. [11] and (b) evolution of Cell 1's voltage and current flowing between Cell 1 and Cell 2's negative electrodes when air and reformate are alternatively fed to the negative compartments. (N.B.: Current is positive when it flows from Cell 2's negative electrode to Cell 2's negative electrode).

Tang et al. [11] considered that the results presented in Fig. 12(b) were representative of "reverse current decay mechanism". However, an alternative explanation could be provided by considering the behavior of an electric circuit integrating a generator and an electrolysis cell connected in series. The current flowing from the generator to the electrolyzer cell can be determined as follow by the combination of equations (26)–(28):

$$i = \frac{(U_{\mathrm{eq},1} - U_{\mathrm{eq},2}) - (\eta_1 + \eta_2)}{r_1 + r_2 + r_{\mathrm{wiring}}} = \frac{(U_{\mathrm{eq},1} - \eta_1) - (U_{\mathrm{eq},2} + \eta_2)}{r_1 + r_2 + r_{\mathrm{wiring}}} \quad (31)$$

with:

$$\eta_i = \eta_{i,\mathrm{a}} + |\eta_{i,\mathrm{c}}| \quad (32)$$

At the beginning of the experiment and according to Eq. (31), as far as $(U_{\mathrm{eq},1} - \eta_1) > (U_{\mathrm{eq},2} - \eta_2)$, the current will be positive and Cell 1 behaves as generator while Cell 2 will behave as electrolyzer. In the opposite case, the current in Eq. (31) will be negative and will therefore flow in the opposite direction. Then, Cell 2 will behave as generator while Cell 1 will behave as electrolyzer. The change in current flow direction is explained by the change in the composition of the gas flowing in the negative compartments. Indeed, as air is fed in Cell 1, it pushes away the reformate it contained which enters Cell 2. As a consequence, Cell 1's voltage progressively decreases as negative electrode's potential increases due to the formation of a mixed potential (cf. Section 2.5) associated with the progression of the air/fuel front. Fig. 6 can give an image of the evolution of Cell 1's negative electrode potential while hydrogen partial pressure decreases as the air/reformate front progresses. In addition, reformate pushed away from Cell 1 pushes in turn away the air that was previously present in Cell 2. As a consequence, Cell 2's negative potential decreases and therefore its voltage increases. When sufficient amount of air entered Cell 1's negative compartment and sufficient amount of reformate entered Cell 2's negative compartment, $(U_{\mathrm{eq},2} + \eta_2)$ becomes higher than $(U_{\mathrm{eq},1} - \eta_1)$ and current reverses. It further increases in magnitude as reformate coming from Cell 1, after being pushed away by the air, fills Cell 2. Once Cell 2 is completely filled with reformate, air coming from Cell 1 starts entering Cell 2 and current decreases back again, due to the decrease of Cell 2's voltage associated with the increase of its negative electrode potential. Once both cells are completely filled with air, their voltage is equal and current is zero. Once reformate is refilled again in Cell 1 (Case 2 in Fig. 12(b)), $(U_{\mathrm{eq},1} - \eta_1)$ rise rapidly and current flows again in the same direction than at the very beginning of the experiment. It further decreases back once Cell 1 is completely filled with reformate and reformate fills Cell 2. The small current reversal, associated with a small Cell 1's voltage decrease might be explained by a higher Cell 2's transient voltage due to potential hydrogen permeation in Cell 1. At the equilibrium, both cell voltages are equal and current is zero. Our analysis seems to be confirmed by the authors who observed that cell 2's positive electrode's electrochemical area loss after 50 cycles is similar with the one observed on an equivalent cell galvanostatically aged at 2 mA cm^{-2}.

Siroma et al. [129] also aimed at validating the "reverse current decay mechanism" by using a single cell with a 97-fold segmented electrode, completely electronically insulated (both current col-

lector and gas diffusion electrode were segmented), and amongst which three were used as reference. These segments were distributed like honeycomb cells at the electrode surface.

Segments were all connected to each other by a zero-shunt current/voltage converter while counter electrode was left unconnected. They performed three different experiments to simulate a moving air fuel/front prior to cell start-up. They mapped the current flowing in each segment at OCV and followed the evolution of counter-electrode and some neighboring segments potential vs. each reference electrode. According to their description, when the air/fuel front was moving in the compartment containing the segmented electrode, they observed that, in air rich regions, current was flowing out of the cell (current was positive) while, in fuel rich regions, current was flowing to the cell (current was negative). Therefore, electrons are flowing from hydrogen rich regions towards air rich regions, which is consistent with a mixed current with HOR as anodic component and ORR as cathodic component (cf. Section 2.5).

4.2.1.3. Conclusions on local fuel starvation. Based on previous analysis of literature data, an alternative degradation mechanism can be proposed to the well admitted "reverse current decay mechanism". Indeed, this latter mechanism seems unlikely to occur at single cell level, mainly because it assumes a cell reversal that, as explained in Section 3 and more specifically by Eq. (22), could not occur (even locally) without infringing the basic principles of thermodynamics. Indeed, according to Eq. (22), a cell reversal requires the presence of an external energy supply since it can only occurs if the variation in Gibbs free energy is positive. This external energy supply could either be the equipment used for the experiment or a cell with higher voltage operating as generator [11,121] to which the degrading cell is connected in series, therefore operating in electrolysis mode.

As previously explained, the combination of mixed potential (associated with simultaneous presence of hydrogen and air at the same electrode surface) and current distribution heterogeneity effects can interpret the published experimental results and explain the degradations observed during fuel starvation. Indeed, the electrochemical potential reached at oxygen electrodes in areas where almost no current flow due to heterogeneities in its distribution are high enough to initiate Pt and/or carbon corrosion.

To figure out the correct explanation to the degradations occurring in a single cell under fuel starvation conditions, we would suggest a discriminating experiment. This experiment would be based on a segmented electrode cell similar with the one described by Siroma et al. [129] but in which all the segments would be connected to the electronic load in a single point. Indeed, in addition to a mapping of the current distribution, this set-up, through the electronic insulation between each segment, would allow determining the direction of the current flowing from/to the cell, and particularly the mixed current at OCV. However, the connection of all these segments to a single pole of the electronic load is a key point to guarantee that the current distribution really depends on the heterogeneities in conductivities and polarizations inside the cell. This experimental cell would also favorably benefit from embedded reference electrodes, as described by Baumgartner et al. [35], to measure electrochemical potential distribution at the hydrogen electrode/membrane interface. Last but not least, a specific and meticulous attention will have to be paid to be certain that the equipment used for current and potential control would not provide any energy to the cell. Therefore, strict current sink (electronic load) will have to be used or, at worst, potentiostat equipments should not be allowed to provide current to the cell.

From this suggested experiment set-up, possible cell reversals could be undoubtfully measured and correlated with corresponding current and electrochemical potential distribution heterogeneities, therefore validating or negating the "reverse current decay mechanism".

4.2.2. Overall starvation

In case of complete fuel starvation, the amount of fuel supplied inside one (or more) cell in a stack decreases to a point where starvation appears. Their corresponding voltage progressively fall down [8,37,39] due to mass transfer limitation of HOR. All mechanisms and consequences of local fuel starvation that were previously explained also occur during overall starvation. At single cell level, without external energy supply, the cell voltage falls down to zero and both electrodes exhibit electrochemical potentials close to the one that would prevail at the positive electrode at OCV. Therefore, all Pt and carbon corrosion phenomena, usually occurring during long stay at OCV and described in Sections 2.2.3 and 2.2.4, could occur [97].

In addition, at stack level, when complete fuel starvation occurs, corresponding cells are not anymore able to deliver, through the hydrogen oxidation reaction, the total amount of current driven by the other "normally operating" cells. However, since fuel cell stacks usually operate in galvanostatic mode and since the single cells are all connected in series, a starving cell can be forced to operate at the fixed current by those located upstream from it. These upstream normally operating cells will therefore make it operate in electrolysis mode by providing the needed energy. As a consequence, starving cells' individual voltages exhibit negative values and their anode potential will increase until reaching a value at which other oxidation reactions could occur in order to provide the remaining needed amount of current [8,39,118]. Depending on reached potential value [31,35,122,124], these reactions can be Pt dissolution (Eq. (11)), carbon corrosion (Eq. (13)) and even water electrolysis [29,130]. In these cells, protons produced by water oxidation reaction (reversal reaction of Eq. (2)) cross the membrane towards the cathode, where they are reduced back into hydrogen (reverse reaction of Eq. (1)) [130] Such cell reversal is a rapid source of irreversible degradations [33,121] and could only be detected by an individual cell voltage survey.

4.3. Oxidant starvation

A consequence of oxidant starvation according to Taniguchi et al. [9] is a rapid cell reversal. However, unlike the increase of hydrogen electrode potential above the oxygen electrode's equilibrium potential observed in case of fuel starvation, an oxidant starvation induces a decrease of oxygen electrode potential below hydrogen electrode's equilibrium potential. Taniguchi et al. [9] indeed observed that oxygen electrode potential rapidly dropped to slightly negative value 3 s after experiment start-up, while hydrogen electrode potential remained constant at 0.1 V.

Natarajan et al. [38] investigated the local current density distribution over 4 h at various oxidant flow rates and different temperatures. The main observed consequence of an oxidant starvation is a drop of the reaction rate and current densities in segment downstream.

Liu et al. [39] measured the current distribution during oxygen starvation and observed a progressive decrease of the local current density in the affected region, indicating that the oxidant is unevenly distributed on the catalytic surface, while the non-affected region remains insensitive to starvation.

5. Failure prevention

5.1. Fault tree analysis

As described previously, catalyst layer degradation impacts negatively the cell voltage; but a given defect might be associated with

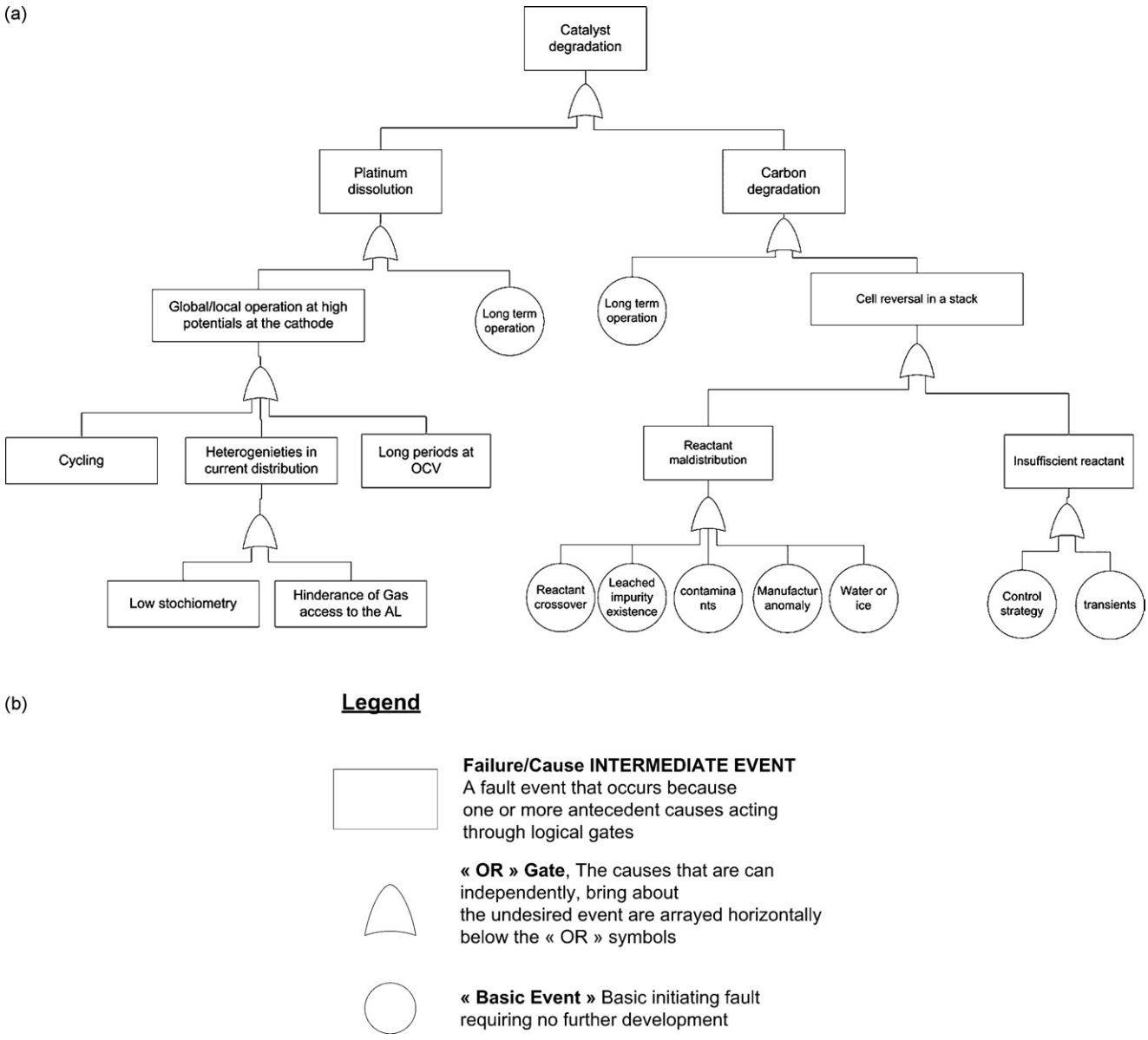

Fig. 13. (a) Fault tree associated with catalyst degradation, (b) legend.

several degradation modes and a given degradation mode can generate several consequences on the fuel cell. To clear out the different contributions, we will use an analysis tool widely used in operating safety and reliability science: the Fault Tree Analysis (FTA) [131]. A fault or failure tree is a graphical representation of the relationship between an undesirable event (called a top event) and all its potential causes. It is a "top-down" approach to failure analysis starting with the top event (failure, malfunction . . .) and determines all the causes that can lead to it. The analysis proceeds by determining how these top events can be caused by individual or combined lower level failures or events. FTA is a formal methodology for determining the combinations of the component level failures that could result in the occurrence of specific failures at a system level.

In our case, the catalyst degradation is the top event. Corresponding failure tree is reported in Fig. 13. To prevent the occurrence of this failure, we need on one hand to detect them and on the other to define an appropriate mitigation strategy.

Table 1 summarizes the PEM failures linked to starvation and catalyst degradation as well as the potential causes, symptoms and characterization methods in literature.

5.2. Existing diagnostic methods

As explained in Sections 3 and 4, degradation can either occurs during long-term ageing or during a sudden uncontrolled operating condition, like a reactant starvation, and the latter generally induces more permanent degradations than the former and within very short time. That is why, early diagnostic of this faulty mode of operation is necessary.

As said before, under fuel starvation, the cell voltage will decrease to small or, inside a stack, even to negative values. In this case, the starvation is relatively easy to detect by monitoring voltages of individual cells or groups of cells, as patented by Ballard Power Systems. [132] Other methods widely reported in the literature to detect a cell starvation are based on current distribution monitoring inside individual cells, which requires preliminary electrode segmentation [31,35,37,39,122,124]. However, due to its complexity, this method is of little interest for monitoring a complete fuel cell stack in operation.

Several characterization methods can be combined: polarization curve (for individual cells or overall fuel cell) [39], temperature dis-

Table 1
Summary of the PEM faults linked to catalyst degradation and characterization methods in literature.

Issue	Potential cause	Indication/symptom	Characterization/diagnostic technique
Pt dissolution and agglomeration	- Starvation	Loss of the catalytic active surface	TEM, EDX, CV
	- Ageing	Presence of catalyst particles in the exhaust water	Analysis of the exhaust
	- Cycling conditions	Increase of particles size	
Carbon corrosion	- Fuel and oxidant starvation:	Uneven current distribution (negative values)	Segmented electrode
	- Flooding, uneven reactants supply	Observation of temperature distribution	Segmented electrode
	- GDL or flow channels obstruction. . .	Increase of the individual cell voltages dispersion and including negative values [120]	Individual cell voltage monitoring
	- Cycling conditions (cathode)	Inversed flow at the fuel outlet [122]	Sensing the flow direction
	- Start-up/shutdown (anode)	Detect C, CO and CO_2 at the exhaust [12,31,35]	Analysis of the exhaust
Starvation	- Flooding	Uneven current distribution (negative values)	Segmented electrode
	- Insufficient reactants supply	Observation of temperature distribution	Segmented electrode
	- Uneven reactants supply (GDL or flow channels obstruction)	Dispersion of individual cell voltage	Individual cell voltage monitoring
		Increase of the individual cell voltages dispersion and including negative values [120]	Individual cell voltage monitoring
		Inversed flow at the fuel outlet	Sensing the flow direction pressure drop, outlet flow sensing
		Presence of "Vacuum effect" [132]	

tribution analysis, detection of CO_2 gas in cathodic compartment's exhaust (to detect carbon corrosion) as well as sensing the direction of the electrode outlet flow [123]. This last method was patented by Reiser [123] and is predicated on the observation that no starvation could occur as long as the exhaust gas flows out the stack assembly towards ambient. A controller disconnects the fuel cell load in the case of opposite outward flow direction. Unfortunately, this method cannot detect a fuel starvation caused by oxygen permeation into the anode.

In case of fuel leakages, Kim et al. [133] observed unstable oscillations and "vacuum effect": the fuel remaining in the manifold and the ambient air are drawn into the cell in order to equilibrate the pressure. Similarly, Natarajan et al. [37] observed, by routing the hydrogen exit through a long vertical tubing with one end placed in a water reservoir, that the pressure near the exit of anode channel dropped below atmospheric and that the water in the reservoir rose in the tubing to accommodate this drop. This procedure also prevented ambient air from being sucked into the anode chamber.

In case of partial fuel starvation described in Section 4.2.1, the detection is difficult, since the potential is decreased locally whereas the overall potential remains in an acceptable range. Therefore monitoring the individual cell voltages does not allow detecting a localized starvation as described by Reiser et al. [121].

5.3. Mitigation, prevention

The catalyst degradation can be mitigated by a wise control of operating parameters such as pressures, cell temperature, humidity levels, current density [12]. Following proper control strategies and choosing adequate anode structure, catalyst and electrode materials play also a great role in limiting the damages caused by all the kind of degradations cited above. At the anode, for instance, Knights et al. [118] and Wilkinson et al. [134] proposed to reduce catalyst degradation by favoring oxidation of water over carbon through a modification of anode structure:

- enhance water retention in the anode by adding or modifying the PTFE and/or ionomer, adding water blocking components such as graphite;
- use improved catalysts in order to reduce the required anode potential for water electrolysis and thus the associated carbon oxidation (additional Ru in the anode);
- use more robust catalyst support like graphitic carbon or alternative support material.
- increase catalyst surface coverage on the support to reduce the carbon contact area with the reactants.

To limit cell performance degradation, the cathode structure could also be modified by increasing its GDL's porosity which would modify locally the gases diffusion or by using materials that enhance oxygen and water mass transfers [134].

Some patents and papers [123,135,136] focused on fuel cell starvation. They are more related to the starvation prevention than to the mitigation of its effects; trying to avoid the occurrence of starvation since it causes irreversible damages to the cell: The best mitigation is careful cell-stack design and controls to ensure uniform fuel distribution. Some procedures to shut-down a FC in order to avoid fuel starvation have also been described. Van dine et al. [137] proposed the following sequence: disconnecting the primary load from the external circuit, stopping the air flow to the cathode while applying an auxiliary resistive load in order to decrease the cathodic potential and maintain the anodic potential at low values. In order to sustain important current demands or sudden load changes, Vahidi et al. [135] used an ancillary power source with fast response time (an ultracapacitor) charged by the fuel cell during normal operation, to provide current during the periods when the fuel cell is unable to follow the demand.

However, as shown by Ballard Power Systems [18], operating in perfectly controlled starvation conditions can be beneficial. Their method and apparatus use periodic transient starvation at the anode to oxidize and remove the catalyst poisons. This method has a real competitive advantage over classical "Anode cleaning" methods such as purging, which require the cell to stop, because the fuel cell is still operating and provide power.

6. Conclusion

The degradation of PEMFC Pt-based catalyst can be categorized in two classes: the catalyst metal degradation and the carbon-support corrosion. In addition, these degradations can either occur during long-term ageing, during transient operation or after an incident. In the first case, catalyst degradation is a continuous process that will affect fuel cell performance and durability. In the latter case, degradations are usually irreversible and can even dramatically reduce the fuel cell lifetime.

Fuel starvation is one of the most critical faulty operation and its prevention requires proper reactant feeding and distribution. Heterogeneities in current distribution can induce local fuel starvations

which locally increase electrochemical potentials at oxygen electrode, thus promoting carbon and Pt metal corrosion. Moreover, at stack level, a complete fuel starvation can induce even worst degradations since the cells connected in series upstream from the starving cells can make them operating in electrolysis mode, enhancing carbon and Pt corrosion. However, such cell reversal seems unlikely to occur at single cell level since it would require an external energy supply to the system, which seems impossible when it operates in fuel cell mode. In addition, the degradations observed in single cells during fuel starvation could be alternatively explained by a combination of mixed potential (associated with simultaneous presence of hydrogen and air at the same electrode surface) and current distribution heterogeneity effects. The electrochemical potential reached at oxygen electrodes in the areas where almost no current flow (due to heterogeneities in its distribution) are high enough to initiate Pt and/or carbon corrosion. To figure out which mechanism rules the single cell behavior during fuel starvation, a discriminating experiment has been proposed.

Finally, a diagnostic approach should be preferred to mitigation strategies since it is almost impossible to mitigate the consequences of a starvation due to their irreversibility. However, such tools (individual cell voltage or current distribution monitoring) are not easy to implement in a fuel cell system on the field.

Acknowledgements

The authors would like to thank the French National Research Agency (ANR), in the scope of its national action plan for hydrogen (PAN-H) for financially supporting this work.

References

[1] DOE "Department of Energy", http://www.sc.doe.gov/bes/hydrogen.pdf, accessed on: 02/02/2009.
[2] S. Zhang, X. Yuan, H. Wang, W. Mérida, H. Zhu, J. Shen, S. Wu, J. Zhang, Int. J. Hydrogen Energy 34 (2009) 388–404.
[3] W. Bi, T.F. Fuller, J. Electrochem. Soc. 155 (2008) B215–B221.
[4] W. Schmittinger, A. Vahidi, J. Power Sources 180 (2008) 1–14.
[5] Y. Shao, G. Yin, Y. Gao, J. Power Sources 171 (2007) 558–566.
[6] N. Yousfi-Steiner, P. Moçotéguy, D. Candusso, D. Hissel, A. Hernandez, A. Aslanides, J. Power Sources 183 (2008) 260–274.
[7] M. Schulze, T. Knöri, A. Schneider, E. Gülzow, J. Power Sources 127 (2004) 222–229.
[8] A. Taniguchi, T. Akita, K. Yasuda, Y. Miyazaki, J. Power Sources 130 (2004) 42–49.
[9] A. Taniguchi, T. Akita, K. Yasuda, Y. Miyazaki, Int. J. Hydrogen Energy 33 (2008) 2323–2329.
[10] V.O. Mittal, H.R. Kunz, J.M. Fenton, Electrochem. Solid State Lett. 9 (2006) A299–A302.
[11] H. Tang, Z. Qi, M. Ramani, J.F. Elter, J. Power Sources 158 (2006) 1306–1312.
[12] S. Maass, F. Finsterwalder, G. Frank, R. Hartmann, C. Merten, J. Power Sources 176 (2008) 444–451.
[13] B. Wahdame, D. Candusso, F. Harel, X. François, M.-C. Péra, D. Hissel, J.-M. Kauffmann, J. Power Sources 182 (2008) 429–440.
[14] X. Yan, M. Hou, L. Sun, H. Cheng, Y. Hong, D. Liang, Q. Shen, P. Ming, B. Yi, J. Power Sources 163 (2007) 966–970.
[15] X. Cheng, Z. Shi, N. Glass, L. Zhang, J. Zhang, D. Song, Z.-S. Liu, H. Wang, J. Shen, J. Power Sources 165 (2007) 739–756.
[16] A. Collier, H. Wang, X. Zi Yuan, J. Zhang, D.P. Wilkinson, Int. J. Hydrogen Energy 31 (2006) 1838–1854.
[17] J. Stumper, M. Lohr, S. Hamada, J. Power Sources 143 (2005) 150–157.
[18] J. St Pierre, D.P. Wilkinson, S. Knights, M.L. Bos, J. New Mater. Electrochem. Syst. 3 (2000) 99–106.
[19] W. He, G. Lin, T.V. Nguyen, AIChE J. 49 (2003) 3221–3228.
[20] D. Di Penta, K. Bencherif, Q.H. Zhang, M. Sorine, Proc. 2006 IEEE Int. Conf. Control Appl. 1–4 (2006) 1529–1534.
[21] R.M. Darling, J.P. Meyers, J. Electrochem. Soc. 152 (2005) A242–A247.
[22] E. Guilminot, A. Corcella, F. Charlot, F. Maillard, M. Chatenet, J. Electrochem. Soc. 154 (2007) B96–B105.
[23] K. Ota, Y. Koizumi, S. Mitsushima, N. Kamiya, ECS Meet. Abstr. 602 (2006) 556–1556.
[24] X. Wang, R. Kumar, D.J. Myers, Eletrochem. Solid-State Lett. 9 (2006) A225–A227.
[25] M.S. Wilson, F.H. Garzon, K.E. Sickafus, S. Gottesfeld, J. Electrochem. Soc. 140 (1993) 2872–2877.
[26] W. Bi, G.E. Gray, T.F. Fuller, Eletrochem. Solid-State Lett. 10 (2007) B101–B104.
[27] K. Yasuda, A. Taniguchi, T. Akita, T. Ioroi, Z. Siroma, Phys. Chem. Chem. Phys. 8 (2006) 746–752.
[28] M.L. Perry, T. Patterson, C. Reiser, ECS Trans. Chem. Lett. 3 (2006) 783–795.
[29] J.P. Meyers, R.M. Darling, J. Electrochem. Soc. 153 (2006) A1432–A1442.
[30] T. Fuller, G. Gray, ECS Trans. 1 (2006) 345–353.
[31] W.R.R. Baumgartner, W.R.R. Baumgartner, E. Wallnofer, T. Schaffer, V. Hacker, V. Peinecke, P. Prenninger, ECS Trans. 3 (2006) 811–825.
[32] P.T. Yu, W. Gu, R. Makharia, F.T. Wagner, H.A. Gasteiger, ECS Trans. 3 (2006) 797–809.
[33] T.W. Patterson, R.M. Darling, Eletrochem. Solid-State Lett. 9 (2006) A183–A185.
[34] P. Thounthong, P. Sethakul, Power Conversion Conference: PCC'07, Nagoya, 2007.
[35] W.R. Baumgartner, P. Parz, S.D. Fraser, E. Wallnofer, V. Hacker, J. Power Sources 182 (2008) 413–421.
[36] Z.Y. Liu, B.K. Brady, R.N. Carter, B. Litteer, M. Budinski, J.K. Hyun, D.A. Muller, J. Electrochem. Soc. 155 (2008) B979–B984.
[37] D. Natarajan, T.V. Nguyen, AIChE J. 51 (2005) 2587–2598.
[38] D. Natarajan, T.V. Nguyen, AIChE J. 51 (2005) 2599–2608.
[39] Z. Liu, L. Yang, Z. Mao, W. Zhuge, Y. Zhang, L. Wang, J. Power Sources 157 (2006) 166–176.
[40] J.T. Pukrushpan, A.G. Stefanopoulou, P. Huei, IEEE 24 (2004) 30–46.
[41] X. Liu, H. Guo, F. Ye, C.F. Ma, Electrochim. Acta 52 (2007) 3607–3614.
[42] D. Hissel, M.C. Pera, J.M. Kauffmann, J. Power Sources 128 (2004) 239–246.
[43] J. Larminie, A. Dicks, Fuel Cell System Explained, 1st ed., John Wiley & Sons, 2000.
[44] X. Yu, S. Ye, J. Power Sources 172 (2007) 145–154.
[45] J. Wang, G. Yin, Y. Shao, S. Zhang, Z. Wang, Y. Gao, J. Power Sources 171 (2007) 331–339.
[46] K. Ruth, M. Vogt, R. Zuber, in: W. Vielstich, A. Lamm, H. Gasteiger (Eds.), Handbook of Fuel Cells: fundamentals technology and applications, Wiley, England, 2003, pp. 489–496.
[47] D. Thompsett, in: W. Vielstich, A. Lamm, H. Gasteiger (Eds.), Handbook of Fuel Cells: fundamentals technology and applications, Wiley, England, 2003, pp. 467–480.
[48] S. Schuldiner, T.B. Warner, B.J. Piersma, J. Electrochem. Soc. 114 (1967) 343–349.
[49] J.P. Diard, B. Le Gorrec, C. Montella, Cinétique electrochimique, "Hermann editions", Paris, 1996.
[50] A. Damjanovic, A. Dey, J.O.M. Bockris, Electrochim. Acta 11 (1966) 791–814.
[51] S. Schuldiner, R.M. Roe, J. Electrochem. Soc. 110 (1963) 332–338.
[52] R. Thacker, J.P. Hoare, J. Electroanal. Chem. 30 (1971) 1–14.
[53] H. Wroblowa, M.L.B. Rao, A. Damjanovic, J.O.M. Bockris, J. Electroanal. Chem. 15 (1967) 139–150.
[54] A. Damjanovic, V. Brusic, Electrochim. Acta 12 (1967) 615–628.
[55] D.B. Sepa, M.V. Vojnovic, A. Damjanovic, Electrochim. Acta 26 (1981) 781–793.
[56] H. Xu, Y. Song, H.R. Kunz, J.M. Fenton, J. Electrochem. Soc. 152 (2005) A1828–A1836.
[57] J.P. Hoare, J. Electrochem. Soc. 109 (1962) 858–865.
[58] T. Yoda, H. Uchida, M. Watanabe, Electrochim. Acta 52 (2007) 5997–6005.
[59] E. Guilminot, A. Corcella, M. Chatenet, F. Maillard, F. Charlot, G. Berthome, C. Iojoiu, J.Y. Sanchez, E. Rossinot, E. Claude, J. Electrochem. Soc. 154 (2007) B1106–B1114.
[60] S. Mitsushima, S. Kawahara, K.-i. Ota, N. Kamiya, J. Electrochem. Soc. 154 (2007) B153–B158.
[61] A.V. Virkar, Y. Zhou, J. Electrochem. Soc. 154 (2007) B540–B547.
[62] S. Motupally, International Workshop on Degradation Issues in Fuel Cells, Crete, Greece, September 19–21, 2007.
[63] T.A. Zawodzinski, J. Davey, J. Valerio, S. Gottesfeld, Electrochim. Acta 40 (1995) 297–302.
[64] J. Zhang, B.A. Litteer, W. Gu, H. Liu, H.A. Gasteiger, J. Electrochem. Soc. 154 (2007) B1006–B1011.
[65] R. Makharia, M.F. Mathias, D.R. Baker, J. Electrochem. Soc. 152 (2005) A970–A977.
[66] S.C. Ball, S.L. Hudson, D. Thompsett, B. Theobald, J. Power Sources 171 (2007) 18–25.
[67] Y. Shao-Horn, P. Ferreira, O.G.J. la, R. Makharia, S. Kocha, H. Gasteiger, ECS Meet. Abstr. 502 (2006) 1182.
[68] Y. Shao-Horn, P. Ferreira, O.G.J. la, D. Morgan, H.A. Gasteiger, R. Makharia, ECS Trans. 1 (2006) 185–195.
[69] M. Fowler, R.F. Mann, J.C. Amphlett, B.A. Peppley, P.R. Roberge, in: W. Vielstich, H.A. Gasteiger, A. Lamm (Eds.), Handbook of Fuel Cells: Fundamentals Technology and Applications, vol. 3, John Wiley & Sons, England, 2003, pp. 663–677.
[70] M. Mathias, H. Gasteiger, R. Makharia, S. Kocha, T. Fuller, J. Pisco, Abstr. Pap. Am. Chem. Soc. 228 (2004), 002-FUEL.
[71] R. Makharia, S. Kocha, P. Yu, C. Gittleman, D. Miller, C. Lewis, F. Wagner, H. Gasteiger, ECS Meet. Abstr. 502 (2006) 1165.
[72] L.M. Roen, C.H. Paik, T.D. Jarvi, Eletrochem. Solid-State Lett. 7 (2004) A19–A22.
[73] J. Willsau, J. Heitbaum, J. Electroanal. Chem. 161 (1984) 93–101.
[74] R.L. Borup, J.R. Davey, F.H. Garzon, D.L. Wood, M.A. Inbody, J. Power Sources 163 (2006) 76–81.
[75] C.H. Hamann, A. Hamnett, W. Vielstich, Electrochemistry, Wiley VCH, Weinheim, 2007.
[76] H.H. Girault, Electrochimie Physique et Analytique, Presses Polytechniques et Universitaires Romandes, Lausanne, 2007, pp. 61–63.

[77] F. Miomandre, S. Sadki, P. Audebert, R. Méallet-Renault, Electrochimie, des Concepts aux Applications, "Dunod", Paris, 2005.
[78] H. Gorgun, M. Arcak, F. Barbir, J. Power Sources 157 (2006) 389–394.
[79] F. Barbir, H. Gorgun, X. Wang, J. Power Sources 141 (2005) 96–101.
[80] M.A. Rubio, A. Urquia, S. Dormido, J. Power Sources 171 (2007) 670–677.
[81] F. Barbir, X. Wang, H. Gorgun, ASME Conf. Proc. (2005).
[82] J.M. Le Canut, R.M. Abouatallah, D.A. Harrington, J. Electrochem. Soc. 153 (2006) A857–A864.
[83] F. Barbir, in: A.P. Kakaç, L. Vasiliev (Eds.), Mini-Micro Fuel Cells, Springer, 2008, pp. 13–26.
[84] D. Devilliers, E. Mahé, l'Actualité chimique 1 (2003) 31–40.
[85] C.Z. He, S. Desai, G. Brown, S. Bollepalli, Electrochem. Soc. Interface 14 (2005) 41–44.
[86] S.K. Zecevic, J.S. Wainright, M.H. Litt, S.L. Gojkovic, R.F. Savinell, J. Electrochem. Soc. 144 (1997) 2973–2982.
[87] D.S. Gnanamuthu, J.V. Petrocelli, J. Electrochem. Soc. 114 (1967) 1036–1041.
[88] D.B. Sepa, M.V. Vojnovic, L.M. Vracar, A. Damjanovic, Electrochim. Acta 31 (1986) 91–96.
[89] O. Antoine, Y. Bultel, R. Durand, J. Electroanal. Chem. 499 (2001) 85–94.
[90] A. Parthasarathy, B. Dave, S. Srinivasan, A.J. Appleby, C.R. Martin, J. Electrochem. Soc. 139 (1992) 1634–1641.
[91] A. Parthasarathy, C.R. Martin, S. Srinivasan, J. Electrochem. Soc. 138 (1991) 916–921.
[92] A. Parthasarathy, S. Srinivasan, A.J. Appleby, C.R. Martin, J. Electrochem. Soc. 139 (1992) 2856–2862.
[93] A. Parthasarathy, S. Srinivasan, A.J. Appleby, C.R. Martin, J. Electrochem. Soc. 139 (1992) 2530–2537.
[94] A. Parthasarathy, S. Srinivasan, A.J. Appleby, C.R. Martin, J. Electroanal. Chem. 339 (1992) 101–121.
[95] P. Rodatz, F. Buchi, C. Onder, L. Guzzella, J. Power Sources 128 (2004) 208–217.
[96] N. Perez, Electrochemistry and Corrosion Science, Kluwer Academic, Massachusetts, 2004.
[97] J. Zhang, Y. Tang, C. Song, J. Zhang, H. Wang, J. Power Sources 163 (2006) 532–537.
[98] Y.J. Kim, W.H. Hong, S.I. Woo, H.K. Lee, J. Power Sources 159 (2006) 491–500.
[99] F. Liu, C.-Y. Wang, J. Electrochem. Soc. 154 (2007) B514–B522.
[100] S.C. Thomas, X. Ren, S. Gottesfeld, P. Zelenay, Electrochim. Acta 47 (2002) 3741–3748.
[101] R. Bouchet, E. Siebert, G. Vitter, J. Electrochem. Soc. 147 (2000) 3548–3551.
[102] R. Bouchet, E. Siebert, G. Vitter, J. Electrochem. Soc. 147 (2000) 3125–3130.
[103] N. Miura, H. Kato, Y. Ozawa, N. Yamazoe, T. Seiyama, Chem. Lett. (1984) 1905–1908.
[104] F. Opekar, J. Electroanal. Chem. 260 (1989) 451–455.
[105] F. Opekar, J. Langmaier, Z. Samec, J. Electroanal. Chem. 379 (1994) 301–306.
[106] S. Rosini, E. Siebert, Electrochim. Acta 50 (2005) 2943–2953.
[107] J. Vermeijlen, L.J.J. Janssen, J. Appl. Electrochem. 23 (1993) 26–31.
[108] M. Murthy, N. Sisofo, 3rd European PEFC Forum, Luzern, Switzerland, 8–4 July, 2005.
[109] E. Cho, J.-J. Ko, H.Y. Ha, S.-A. Hong, K.-Y. Lee, T.-W. Lim, I.-H. Oh, J. Electrochem. Soc. 151 (2004) A661–A665.
[110] T. Smolinka, U. Wittstadt, M. Grünerbel, W. Lehnert, 3rd European PEFC Forum, Luzern, Switzerland, 8–4 July, 2005.
[111] J. Xie, D.L. Wood Iii, D.M. Wayne, T.A. Zawodzinski, P. Atanassov, R.L. Borup, J. Electrochem. Soc. 152 (2005) A104–A113.
[112] R.M. Darling, J.P. Meyers, J. Electrochem. Soc. 150 (2003) A1523–A1527.
[113] J. Xie, D.L. Wood Iii, K.L. More, P. Atanassov, R.L. Borup, J. Electrochem. Soc. 152 (2005) A1011–A1020.
[114] B. Wahdame, D. Candusso, X. François, F. Harel, M.-C. Péra, D. Hissel, J.-M. Kauffmann, Int. J. Hydrogen Energy 32 (2007) 4523–4536.
[115] F. Harel, X. Francois, D. Candusso, M.C. Pera, D. Hissel, J.M. Kauffmann, Fuel Cells 7 (2007) 142–152.
[116] B. Wahdame, D. Candusso, X. Francois, F. Harel, M.C. Pera, D. Hissel, J.M. Kauffmann, Int. J. Hydrogen Energy 32 (2007) 4523–4536.
[117] S. Escribano, A. Morin, S. Solan, B. Sommacal, P. Capron, I. Rougeaux, G. Gébel, 3rd European PEFC Forum, Luzern, Switzerland, 8–4 July, 2005.
[118] S.D. Knights, K.M. Colbow, J. St-Pierre, D.P. Wilkinson, J. Power Sources 127 (2004) 127–134.
[119] D. Liu, S. Case, J. Power Sources 162 (2006) 521–531.
[120] D.A. Stevens, M.T. Hicks, G.M. Haugen, J.R. Dahn, J. Electrochem. Soc. 152 (2005) A2309–A2315.
[121] C.A. Reiser, L. Bregoli, T.W. Patterson, J.S. Yi, J.D. Yang, M.L. Perry, T.D. Jarvi, Eletrochem. Solid-State Lett. 8 (2005) A273–A276.
[122] W.R.R. Baumgartner, E. Wallnfer, T. Schaffer, V. Hacker, V. Peinecke, P. Prenninger, ECS Meet. Abstr. 602 (2006) 600.
[123] C.A. Reiser, Preventing fuel starvation of a fuel cell stack, United States Patent No.: 20050164050 (2005).
[124] V. Hacker, W.R. Baumgartner, E. Wallnöfer, International Workshop on Degradation Issues in Fuel Cells, Hersonessos, Greece, September 19–21, 2007.
[125] S.S. Kocha, J.D. Yang, J.S. Yi, AICHE J. 52 (2006) 1916–1925.
[126] A. Hernandez, D. Hissel, R. Outbib, in: D. Hissel (Ed.), IEEE International Symposium on Industrial Electronics, 2006.
[127] F. Coeuret, Ingéniérie des procédés électrochimiques, Ellipses, Paris, 2003.
[128] http://www.zahner.de/workstations.html#specifications, accessed on: 2nd October, 2008.
[129] Z. Siroma, N. Fujiwara, T. Ioroi, S.-i. Yamazaki, H. Senoh, K. Yasuda, K. Tanimoto, J. Power Sources 172 (2007) 155–162.
[130] J.A.S. Bett, N.E. Cipollini, T.D. Jarvi, R.D. Breault, Fuel cell having a corrosion resistant and protected cathode catalyst layer, United States Patent 6855453 (2005).
[131] Y. Mortureux, Arbres de défaillance, des causes et d'événement (Eds.), Techniques de l'Ingénieur, pp. 1–24.
[132] R.H. Barton, Cell voltage monitor for a fuel cell stack, United States Patent 6724194 (2004).
[133] S. Kim, S. Shimpalee, J.W. Van Zee, J. Power Sources 135 (2004) 110–121.
[134] D.P. Wilkinson, J. St-Pierre, in: W. Vielstich, A. Lamm, H. Gasteiger (Eds.), Handbook of fuel cells: fundamentals technology and applications, Wiley, England, 2003, pp. 611–626.
[135] A. Vahidi, A. Stefanopoulou, H. Peng, Proceedings of the 2004 American Control Conference, vol. 1–6, 2004, pp. 834–839.
[136] D.P. Wilkinson, C.Y.F. Chow, D.E. Allan Deceased, P.J. Allan, E.P. Johannes, J.A. Roberts, J. St-pierre, C.J. Longley, J.K.K. Chan, Method and apparatus for operating an electrochemical fuel cell with periodic fuel starvation at the anode, 6096448 (2000).
[137] L.L. Van Dine, M.M. Steinbugler, C.A. Reiser, G.W. Scheffler, Procedure for shutting down a fuel cell system having an anode exhaust recycle loop, April 2nd, 2003.
[138] Z. Liu, Z. Mao, B. Wu, L. Wang, V.M. Schmidt, J. Power Sources 141 (2005) 205–210.
[139] H. Sun, G. Zhang, L.-J. Guo, H. Liu, J. Power Sources 158 (2006) 326–332.
[140] H. Sun, G. Zhang, L.-J. Guo, S. Dehua, H. Liu, J. Power Sources 168 (2007) 400–407.
[141] T. Hottinen, M. Noponen, T. Mennola, O. Himanen, M. Mikkola, P. Lund, J. Applied Electrochem. 33 (2003) 265–271.